ANOMALOUS DISPERSION IN GASES DERIVED FROM THE OPTICAL DEPTH.

THEORETICAL TREATMENT; LINE BY LINE CALCULATIONS

BY

EGIL SINGEN, BJØRNAR YSTAD

NDRE/PUBL-91/1002

ISSN 0800-4412

FORSVARETS FORSKNINGSINSTITUTT

NORWEGIAN DEFENCE RESEARCH ESTABLISHMENT

P O Box 25 – N-2007 Kjeller, Norway

A-1

ANOMALOUS DISPERSION IN GASES DERIVED FROM THE OPTICAL DEPTH.

THEORETICAL TREATMENT; LINE BY LINE CALCULATIONS

by

EGIL BINGEN, BJØRNAR YSTAD

NDRE/PUBL–91/1002

ISSN 0800–4412

FORSVARETS FORSKNINGSINSTITUTT

NORWEGIAN DEFENCE RESEARCH ESTABLISHMENT

P O Box 25 - N-2007 Kjeller, Norway

June 1991

NORWEGIAN DEFENCE RESEARCH ESTABLISHMENT (NDRE)
FORSVARETS FORSKNINGSINSTITUTT (FFI)

POST OFFICE BOX 25
N-2007 KJELLER, NORWAY

UNCLASSIFIED
SECURITY CLASSIFICATION OF THIS PAGE (when data entered)

REPORT DOCUMENTATION PAGE

1) PUBL/REPORT NUMBER	2) SECURITY CLASSIFICATION	3) NUMBER OF PAGES
NDRE/PUBL-91/1002	UNCLASSIFIED	55
1a) JOB REFERENCE	2a) DECLASSIFICATION/DOWNGRADING SCHEDULE	
603-E/131.1	-	

4) TITLE

ANOMALOUS DISPERSION IN GASES DERIVED FROM THE OPTICAL DEPTH. THEORETICAL TREATMENT; LINE BY LINE CALCULATIONS

5) NAMES OF AUTHOR(S) IN FULL (surname first)
BINGEN Egil, YSTAD Bjørnar

6) DISTRIBUTION STATEMENT

Approved for public release. Distribution unlimited
(Offentlig tilgjengelig)

7) INDEXING TERMS

IN ENGLISH:	IN NORWEGIAN:
a) Anomalous dispersion	a) Anomal dispersjon
b) Gases	b) Gasser
c) Optical depth	c) Optisk dybde
d) Hilbert transform	d) Hilbert transform
Line forms	e) Linje former

THESAURUS REFERENCE:

8) ABSTRACT (continue on reverse side if necessary)

This report describes a theoretical development of the anomalous dispersion in a mixture of gases, from the optical depth. The dispersion is determined by a Hilbert transform of the optical depth. An optical depth formulation as defined by Van Vleck and Huber is fundamental to this treatment. The Hilbert transform is performed without approximations giving an expression for the dispersion which is valid for all wavenumber subject to the validity of the dipole approximation and a classical description of the electromagnetic field. The derived expression is adequate for the Voigt, Lorentz and Doppler line shape functions. The effect of line coupling is not taken into account.

An approximate expression for the dispersion is implemented for line by line calculations of dispersion in a modified FASCOD2. This approximation is valid when homogenous (Lorentz) broadning is dominant

9) DATE	AUTHORIZED BY (This page only)	POSITION
28 Jun 91	E Klippenberg	Director

UNCLASSIFIED
SECURITY CLASSIFICATION OF THIS PAGE (when data entered)

CONTENTS

ANOMALOUS DISPERSION IN GASES DERIVED FROM THE OPTICAL DEPTH
Theoretical treatment; line by line calculations

1 INTRODUCTION

This report describes the high resolution wave number dependence of the refractive index in gases. The wave number dependence of the refractive index is caused by the ability of a gas to absorb and emit electromagnetic radiation. Knowledge of the spectral absorption (or the optical depth) is the basis for refractive index calculations in this report.

The spectral absorption can be calculated from the quantity optical depth. The spectral behavior of the optical depth is mainly described by the spectral line shape function. The correct line shape function is not known, but the approximations of Voigt, Lorentz and Doppler are normally used for calculation of spectral absorption. These approximations will also be used in this report for the refractive index calculations[1]. They give a correct description of the line shape near the resonance wave number but far away from resonance they are not correct. This effect has greater implications on the accuracy of calculated refractive index than calculated absorption due to differences in the spectal behavior.

Line by line calculation of absorption at a certain wave number is normally performed by only taking into account the influence from transitions "nearby" the given wave number. The contribution to the absorption from the "wings" of distant transitions is neglected. This approximate calculation of absorption gives fairly good results because the line shape function falls off rapidly ($\sim(\sigma-\sigma_j)^{-2}$) with the distance from the resonance wave number (σ_j).

---

[1]A correct line shape function would, among other effects, have to take the effect of line coupling into account. This effect will not be discussed in this report.

Line by line calculation of refractive index leads to a somewhat different situation with respect to accuracy than encountered in the calculation of absorption. The reason is that the contribution to the refractive index from the "wings" of distant transitions is much greater due to the slower fall off ($\sim(\sigma-\sigma_j)^{-1}$) with the distance from the resonance wave number. This means that calculation of the refractive index at a given wave number requires that the contribution from the "wings" of <u>all</u> resonance transitions are taken into account. When dealing with atmospheric refractive index especially the contribution from the very strong UV-transitions has to be taken into account both in the visible, infrared and μ-wave part of the spectrum.

A computation of the refractive index as outlined above is not treated in this report although the theoretical results of Chapter 4 are suitable for such computation provided the Voigt or Lorentz line shape function is used. The result from such computation will have limited value due to the validity of the distant "wings" of the line form functions. The computations in this report is performed by only taking into account the contribution to the refractive index from resonance transitions in a limited wave number interval centered around the wave number of interest (i e a procedure analogous to the one described for calculation of absorption). The result from these computations will therefore only give the local wave number dependence of the refractive index; more commonly named the anomalous dispersion due to resonance transitions. This quantity is in this report called the dispersion and is denoted Δn.

For the atmospheric refractive index an empirical formula has been developed by Edlén (1) based on measurements in the visible part of the spectrum. This formula with corrections for atmospheric temperature, humidity and pressure is also widely used for calculation of atmospheric refractive index in the infrared, μ-wave and even radio-wave part of the spectrum. The accuracy of these results is however questionable since the basic measurements are only performed in the visible. It is however reasonable to believe that Edlén's formula expresses the total contribution to the refractive index from the "wings" of distant strong transitions especially the very strong UV-transitions in the atmospheric spectrum. The coarse (low

resolution) wave number dependence of atmospheric refractive index is then described by Edlén's formula whilst the fine structure (high resolution) wave number dependence is described by the dispersion derived in this report. A sum of these two quantities is then an estimate of the total atmospheric refractive index. The contribution to this sum from the dispersion is small in the visible and infrared part of the spectrum. In the wave number region below 400 cm^{-1} the dispersion is important near the resonance transitions. This situation will be demonstrated and discussed in Chapter 6.

The calculations in this report is motivated by the fact that there already exists a computer code performing line by line calculations of the optical depth. The code is named Fast Atmospheric Signature Code (FASCOD), and is developed by the U S Air Force Geophysics Laboratory (AFGL). In Chapter 5 it will be shown how line by line calculations of the dispersion can be performed within the framework of a modified FASCOD.

This report consists of two main parts: A theoretical development of the expression for the dispersion (Chapter 2-4) and an implementation of the theoretical result in FASCOD (Chapter 5-6).

In Chapter 2 it is shown how the dispersion can be expressed in terms of the optical depth by means of the linear susceptibility and the Kramers-Kronig relations. The formulation of the optical depth used in this paper is discussed in Chapter 3. An explicit expression for the dispersion is calculated in Chapter 4.

A theoretical development analogous to the one described in this report is given by Tomiyama (2). The theoretical result in this report has however a more general validity since no approximations are needed during the development. This gives an exact expression for the dispersion when the Voigt, Lorentz or Doppler line shape functions are used.

In Chapter 5 it is shown how the expression for the dispersion can be simplified to facilitate implementation within the framework of FASCOD.

Results from calculated amtospheric dispersion in various wave number regions are presented and discussed in Chapter 6. The calculated results are compared with the measurements of Liebe (3).

2 DISPERSION AND OPTICAL DEPTH

This chapter describes how the dispersion can be expressed in terms of the optical depth by means of the linear susceptibility and the Kramers-Kronig relations.

The linear susceptibility, $\chi(\omega)$, is a complex quantity describing the relationship between an external electric field, $\vec{E}$, and the polarization, $\vec{P}$, that is induced by the electric field. When the medium is isotropic the linear susceptibility is a scalar, and the polarization is given by

$$\vec{P} = \chi(\omega)\vec{E} = (\chi'(\omega) + i\chi''(\omega))\vec{E} \qquad (2.1)$$

where $\chi'(\omega)$ is the real- and $\chi''(\omega)$ the imaginary-part of the susceptibility. ω is the angular frequency.

In this context we shall assume a plane wave propagation for the polarization $\vec{P}$

$$\vec{P} = \tfrac{1}{2}\,\vec{\tilde{P}}\, e^{i(\omega t-\kappa z)} + c.c \qquad (2.2)$$

$\vec{\tilde{P}}$ is the complex magnitude and $\kappa = \kappa'+i\kappa''$ is the complex propagation constant with real part κ' and imagninary part κ''.

The large scale macroscopic phenomena of absorption, emission and dispersion of light are the results of transitions between the various atomic or molecular energy levels. The equation of motion for the electric and polarization fields in an isotropic medium are derived in Pantell (4). When a plane wave solution of the form (2.2) is assumed, the equations of motion gives the following expression for the propagation constant, κ

$$\kappa^2 = \frac{\eta^2\omega^2}{c^2}\left[1 + \frac{\chi(\omega)}{\eta^2}\right] \qquad (2.3)$$

In Equation (2.3) η is the contribution to the propagation constant from transitions outside the frequency interval considered for determination of the susceptibility (i e the transitions that are not taken into account in the calculations). The value of η is equal to unity if the contribution from <u>all</u> transitions in a gas is accounted for in the the determination of the susceptibility.

Equation (2.3) is solved by taking the square root and assuming $(\chi(\omega)/\eta^2) << 1$ so that the expansion $[1+\chi(\omega)/\eta^2]^{1/2} = 1+\chi(\omega)/2\eta^2$ holds (which is the case for other than very strong transitions). The result for the complex propagation constant is

$$\kappa = \kappa' + i\kappa'' = \frac{\eta\omega}{c}\left[1 + \frac{\chi'(\omega)}{2\eta^2}\right] + i\,\frac{\omega\chi''(\omega)}{2\eta c} \qquad (2.4)$$

The real and imaginary part of the propagation constant is then given by:

$$\kappa' = \frac{\eta\omega}{c}\left[1 + \frac{\chi'(\omega)}{2\eta^2}\right] \qquad (2.5)$$

and

$$\kappa'' = \frac{\omega\chi''(\omega)}{2\eta c} \qquad (2.6)$$

Since the optical depth, $k(\omega)$, is defined with reference to the absorption of radiant power it can be shown (4) that the imaginary part of the propagation constant is related to the optical depth by

$$k(\omega) = -2\kappa'' = \frac{\omega\chi''(\omega)}{\eta c} \qquad (2.7)$$

The refractive index, $n(\omega)$, in the medium is defined as the ratio between the phase velocity in empty space, c, and the phase velocity in the medium, v_f. By definition the phase velocity in the medium is

$$v_f = \frac{\omega}{\kappa'} \qquad (2.8)$$

The relation between the refractive index and the real part of the susceptibility is then

$$n(\omega) = \frac{c}{v_f} = \eta + \frac{\chi'(\omega)}{2\eta} \tag{2.9}$$

The dispersion as defined in this report is

$$\Delta n(\omega) = \frac{\chi'(\omega)}{2\eta} \tag{2.10}$$

The Equations (2.7) and (2.10) connecting the imaginary and real part of the susceptibility to respectively optical depth and dispersion, are the fundamental equations in this report.

By using the connections between angular frequency and wave number ($\omega = 2\pi c\sigma$) these equations can be rewritten

$$\Delta n(\sigma) = \frac{1}{2\eta} \chi'(\sigma) \tag{2.11}$$

$$k(\sigma) = - \frac{2\pi\sigma}{\eta} \chi''(\sigma) \tag{2.12}$$

The purpose of this chapter is to express the dispersion in Equation (2.11) by the optical depth in Equation (2.12).

As stated by the Kramer-Kronig relations (4) the real and imaginary part of the susceptibility are Hilbert transformed pairs. Mathematically this can be expressed as

$$\chi'(\sigma) = - H[\chi''(\sigma)] \tag{2.13}$$

$$\chi''(\sigma) = H[\chi'(\sigma)] \tag{2.14}$$

The Hilbert transform, $H[f(x)]$, of a function $f(x)$ is defined by

$$H[f(x)] = \frac{1}{\pi} PP \int_{-\infty}^{\infty} \frac{f(x')}{x'-x} dx' \tag{2.15}$$

where PP means that the principal part of the integral is to be evaluated.

From Equations (2.12) and (2.13) the relationship between the real part of the susceptibility and the optical depth is

$$x'(\sigma) = -H\left[-\frac{n}{2\pi\sigma}\, k(\sigma)\right] = \frac{n}{2\pi} H\left[\frac{k(\sigma)}{\sigma}\right] \qquad (2.16)$$

The Equations (2.11) and (2.16) then establish the following relation between the dispersion and the optical depth

$$\Delta n(\sigma) = \frac{1}{4\pi} H\left[\frac{k(\sigma)}{\sigma}\right] \qquad (2.17)$$

The relationship expressed by Equation (2.17) is the basis for the description throughout the rest of this report.

In order to evaluate the Hilbert transform in Equation (2.17) the explicit wave number dependence of the optical depth must be known. This problem will be addressed in the following chapter.

3 THE OPTICAL DEPTH FORMULATION

This chapter contains a formulation of the optical depth which takes into account the molecular processes of absorption and stimulated emission. The explicit wave number dependence of the optical depth is also described both for the Voigt, Lorentz and Doppler line shape functions. The aim of this chapter is to define that part of the optical depth which has to be Hilbert tranformed in order to calculate the dispersion and to define the Voigt, Lorentz and Doppler dispersion functions.

The optical depth formulation of Van Vleck and Huber (5), will be used in this paper. In this formulation the optical depth $k(\sigma)$ of a mixture of different gases can be expressed in the following form (6)

$$k(\sigma) = \sigma \tanh\left(\frac{\beta\sigma}{2}\right) \sum_{ij} W(m_j)\, \tilde{S}_i(T)\, [f(\sigma,\sigma_i) + f(-\sigma,\sigma_i)] \qquad (3.1)$$

where

$W(m_j)$ - Number density of molecular species m_j (molecule/cm^3)

$\tilde{S}_i(T)$ - Line strength of the i'th transition at the temperature T (cm^2/molecule)

$f(\sigma,\sigma_i)$ - Line shape function (cm)

σ - Wave number (cm^{-1})

σ_i - Resonance wave number for the i'th transition

β - = hc/kT; where T is temperature and hc/k is the second radiation constant (1.4388 cm·K)

The line strength, $\tilde{S}_i(T)$, in Equation (3.1) has a specific value for each resonance transition belonging to the different molecular species in the gas mixture. The temperature dependence of the line strength is given by the assumption of thermal equilibrium; i e a Maxwell-Boltzmann distribution of molecules in the excited states and the associated partition functions.

This formulation of the optical depth satisfies three important properties independent of the line shape function. These properties are satisfied even if the fluctuation dissipation theorem for detailed radiation balance is not (5). The properties satisfied by Equation (3.1) are:

a) The generalized Nyquist theorem; i e transition strengths are preserved, and radiation balance between emission and absorption is satisfied in thermal equilibrium (7).

b) The Kramers-Kronig relations, (5) and (8).

c) The f sum rule; which is equivalent to the validity of the familiar formula (qp-pq) = ih/2π of matrix quantum algebra (5).

This means that Equation (3.1) should be valid for all wave numbers provided the dipole approximation is valid and a classical despription of the radiation field is adequate. The accuracy of the calculated optical depth is only dependent of the quality of the approximate line shape function.

In Chapter 2 the connection between dispersion and optical depth is expressed by Equation (2.17). By introducing the optical depth in Equation (3.1) the dispersion can be expressed by

$$\Delta n(\sigma) = \frac{1}{4\pi} \sum_{ij} W(m_j)\tilde{S}_i(T)[F(\sigma,\sigma_i) + G(\sigma,\sigma_i)] \qquad (3.2)$$

where

$$F(\sigma,\sigma_i) = H[\tanh(\frac{\beta\sigma}{2}) \cdot f(\sigma,\sigma_i)] \tag{3.3}$$

$$G(\sigma,\sigma_i) = H[\tanh(\frac{\beta\sigma}{2}) \cdot f(-\sigma,\sigma_i)] \tag{3.4}$$

$H[\cdot]$ is the Hilbert tranform.

To calculate the Hilbert tranforms described by Equations (3.3) and (3.4) it is necessary to introduce an explicit expression for the line shape function, $f(\sigma,\sigma_i)$.

In order to obtain a theoretical result for the dispersion which contain the influence of both homogeneous and inhomogeneous line broadening mechanisms the Voigt line shape function is used for the theoretical calculations in this report. The Voigt line shape is a convolution of the Lorentz line shape describing homogeneous broadening due to molecular collisions and the Doppler line shape describing inhomogeneous broadening due to the distribution of molecular velocities. The Voigt line shape function is described as

$$f_v(\sigma,\sigma_i) = \sqrt{\frac{\ln 2}{\pi}} \cdot \frac{1}{\alpha_d} \int_{-\infty}^{+\infty} \frac{1}{\pi} \frac{\alpha}{(\sigma-x)^2+\alpha^2} \exp\left[-\ln 2 \left(\frac{x-\sigma_i}{\alpha_d}\right)^2\right]dx \tag{3.5}$$

The Lorentz and Doppler line shape functions are defined by

$$f_\ell(\sigma,\sigma_i) = \frac{1}{\pi} \frac{\alpha}{(\sigma-\sigma_i)^2 + \alpha^2} \tag{3.6}$$

$$f_d(\sigma,\sigma_i) = \sqrt{\frac{\ln 2}{\pi}} \cdot \frac{1}{\alpha_d} \exp\left[-\ln 2 \left(\frac{\sigma-\sigma_i}{\alpha_d}\right)^2\right]dx \tag{3.7}$$

where

α - Lorentz half width (HWHM)

α_d - Doppler half widt (HWHM)

The half widths are dependent of molecular species and the thermodynamic situation in the gas mixture. The Doppler line width is also proportional to the resonance wave number. At standard atmospheric

temperature and pressure the Lorentz line width is normally much greater than the Doppler line width.

The Voigt line shape in Equation (3.5) is easily obtained by a convolution of the Lorentz and Doppler line shapes in Equations (3.6) and (3.7) (regarding the wave number difference $\sigma-\sigma_i$ as free variable) followed by a simple change of variable.

$$\begin{aligned} f_v(\sigma,\sigma_i) &= f_\ell(\sigma-\sigma_i) * f_d(\sigma-\sigma_i) \\ &= \int_{-\infty}^{+\infty} f_\ell(\sigma-\sigma_i-y) \cdot f_d(y)dy \\ &= \int_{-\infty}^{+\infty} f_\ell(\sigma-x) \cdot f_d(x-\sigma_i)dx \end{aligned} \tag{3.8}$$

By using the notation in Equations (3.6) and (3.7) the last expressions in Equation (3.8) can formally be written

$$f_v(\sigma,\sigma_i) = \int_{-\infty}^{+\infty} f_\ell(\sigma,x) \cdot f_d(x,\sigma_i)dx \tag{3.9}$$

The notation in Equation (3.9) means that the variable indicated (with x) in the Lorentz and Doppler line shape functions shall be substituted by the integration variable prior to integrations. This type of notation is convenient at a later stage in this report.

The Voigt line shape functions is within the approximations of Lorentz and Doppler line broadening mechanisms a reasonable description of the line shape (to a certain distance from the line center) for most values of temperature and pressure in a gas mixture. However at two extreme situations the Voigt formula can be simplified since (9)

$$\lim_{\alpha_d \to 0} f_d(\sigma,\sigma_i) = \delta(\sigma-\sigma_i) \tag{3.10}$$

$$\lim_{\alpha \to 0} f_\ell(\sigma,\sigma_i) = \delta(\sigma-\sigma_i) \tag{3.11}$$

where $\delta(\cdot)$ is the Dirac δ-function.

The Equations (3.10), (3.11) and (3.9) leads to the following limits for the Voigt line shape function when the half widths tends to zero

$$\lim_{\alpha_d \to 0} f_V(\sigma,\sigma_i) = f_\ell(\sigma,\sigma_i) \tag{3.12}$$

$$\lim_{\alpha \to 0} f_V(\sigma,\sigma_i) = f_d(\sigma-\sigma_i) \tag{3.13}$$

Equation (3.12) describes a situation where homogeneous (Lorentz) broadening completely dominates over inhomogeneous (Doppler) broadening, i e the high pressure regime. Equation (3.13) describes the low pressure regime when $\alpha_d >> \alpha$. Since the natural line broadening due to spontaneous processes is a homogeneous broadening mechanism Equation (3.13) is only a good approximation for the low pressure regime when the Doppler line width is much greater than the natural line width; $\alpha_d >> \alpha_n$. The natural line width is given by

$$\alpha_n = (c \cdot \tau_n)^{-1} \tag{3.14}$$

where τ_n is the natural lifetime.

To make this theoretical development valid for both the high and low pressure regime the Voigt line shape function is used in Equation (3.2). The fact that $f_V(-\sigma,\sigma_i) = f_V(\sigma -\sigma_i)$ (which is obvious by change of variable in Equation (3.5)) gives the following expression for the dispersion

$$\Delta n(\sigma) = \frac{1}{4\pi} \sum_{ij} W(m_j)\tilde{S}_i(T)[F_V(\sigma,\sigma_i) + F_V(\sigma,-\sigma_i)] \tag{3.15}$$

where

$$F_V(\sigma,\sigma_i) = H[\tanh(\tfrac{\beta\sigma}{2})\, f_V(\sigma,\sigma_i)] \tag{3.16}$$

$$F_V(\sigma,-\sigma_i) = H[\tanh(\tfrac{\beta\sigma}{2})\, f_V(\sigma,-\sigma_i)] \tag{3.17}$$

From the definition of the Hilbert transform in Equation (2.15) and

the Voigt line shape function in Equation (3.5) an explicit expression for Equation (3.16) is

$$F_V(\sigma,\sigma_i) = \sqrt{\frac{\ln 2}{\pi}} \cdot \frac{1}{\alpha_d} \cdot H\left[\tanh\left(\frac{\beta\sigma}{2}\right) \cdot \int_{-\infty}^{+\infty} \frac{1}{\pi} \frac{\alpha}{(\sigma-x)^2+\alpha^2} \cdot \exp\left[-\ln 2 \left(\frac{x-\sigma_i}{\alpha_d}\right)^2\right] dx\right] \tag{3.18}$$

$$= \sqrt{\frac{\ln 2}{\pi}} \cdot \frac{1}{\alpha_d} \int_{-\infty}^{+\infty} \cdot H\left[\tanh\left(\frac{\beta\sigma}{2}\right) \cdot \frac{1}{\pi} \frac{\alpha}{(\sigma-x)^2+\alpha^2}\right] \cdot \exp\left[-\ln 2 \left(\frac{x-\sigma_i}{\alpha_d}\right)^2\right] dx \tag{3.19}$$

The Hilbert transform in Equation (3.19) is given by:

$$F_\ell(\sigma,x) \equiv H\left[\tanh\left(\frac{\beta\sigma}{2}\right) \cdot \frac{1}{\pi} \frac{\alpha}{(\sigma-x)^2+\alpha^2}\right]$$

$$= \frac{1}{\pi} PP \int_{-\infty}^{+\infty} \frac{1}{\sigma'-\sigma} \tanh\left(\frac{\beta\sigma'}{2}\right) \cdot \frac{1}{\pi} \frac{\alpha}{(\sigma'-x)^2+\alpha^2} d\sigma'$$

$$= \frac{1}{\pi} PP \int_{-\infty}^{+\infty} \frac{1}{\sigma'-\sigma} \tanh\left(\frac{\beta\sigma'}{2}\right) \cdot f_\ell(\sigma',x)\, d\sigma' \tag{3.20}$$

The integral in Equation (3.20) will be calculated in Chapter 4 by analytic continuation and complex integration. The high and low pressure limits for the dispersion are found from the limits of Equation (3.16) using (3.12) and (3.13)

$$F_\ell(\sigma,\sigma_i) \equiv \lim_{\alpha_d \to 0} F_V(\sigma,\sigma_i) = \frac{1}{\pi} PP \int_{-\infty}^{+\infty} \frac{1}{\sigma'-\sigma} \tanh\left(\frac{\beta\sigma'}{2}\right) \cdot f_\ell(\sigma',\sigma_i)\, d\sigma' \tag{3.21}$$

$$F_d(\sigma,\sigma_i) \equiv \lim_{\alpha \to 0} F_V(\sigma,\sigma_i) = \frac{1}{\pi} PP \int_{-\infty}^{+\infty} \frac{1}{\sigma'-\sigma} \tanh\left(\frac{\beta\sigma'}{2}\right) \cdot f_d(\sigma',\sigma_i)\, d\sigma' \tag{3.22}$$

The functions $F_V(\sigma,\sigma_i)$, $F_\ell(\sigma,\sigma_i)$ and $F_d(\sigma,\sigma_i)$ will in the rest of this report be called the Voigt-, Lorentz- and Doppler dispersion functions.

A comparison of Equations (3.21) and (3.20) shows that the high pressure limit of the dispersion is readily calculated line by line from Equation (3.15) as soon as the integration in (3.20) is performed and

the variable x is substituted by the resonance wave numbers σ_i. At intermediate pressures the integration described by Equation (3.19) must be performed before a line by line calculation of the dispersion can be evaluated.

A calculation of the integral in Equation (3.19) is difficult within the framework of FASCOD therefore the mumerical examples given in this report will mainly concentrate on the high pressure regime.

4 THE HILBERT TRANSFORM OF THE OPTICAL DEPTH

The purpose of this chapter is to calculate an explicit expression for the dispersion based on the optical depth formulation in Chapter 3 and the Voigt line shape function.

The development in Chapter 3 showed that the following Hilbert transform has to be calculated in order to determine the dispersion.

$$F_\ell(\sigma,x) = \frac{1}{\pi} PP \int_{-\infty}^{+\infty} \frac{1}{\sigma'-\sigma} \tanh\left(\frac{\beta\sigma'}{2}\right) \cdot \frac{1}{\pi} \frac{\alpha}{(\sigma'-x)^2+\alpha^2} d\sigma' \qquad (4.1)$$

By using the notation $F(\sigma')$ for the intergrand in Equation (4.1) the evaluation of the principal part of the integral is by definition

$$F_\ell(\sigma,x) = \frac{1}{\pi} \lim_{\epsilon\to 0} \left\{ \int_{-\infty}^{\sigma-\epsilon} F(\sigma')d\sigma' + \int_{\sigma+\epsilon}^{+\infty} F(\sigma')d\sigma' \right\} \qquad (4.2)$$

To be able to evaluate the integral of Equation (4.1) a continuation into the complex plane will be made. By defining a closed contour of integration it is possible to use the residue theorem from complex analysis to evaluate the integral. The contour of integration which is used here is shown in Figure 4.1. It is called C, and it consists of the curves Γ,Γ' and I.

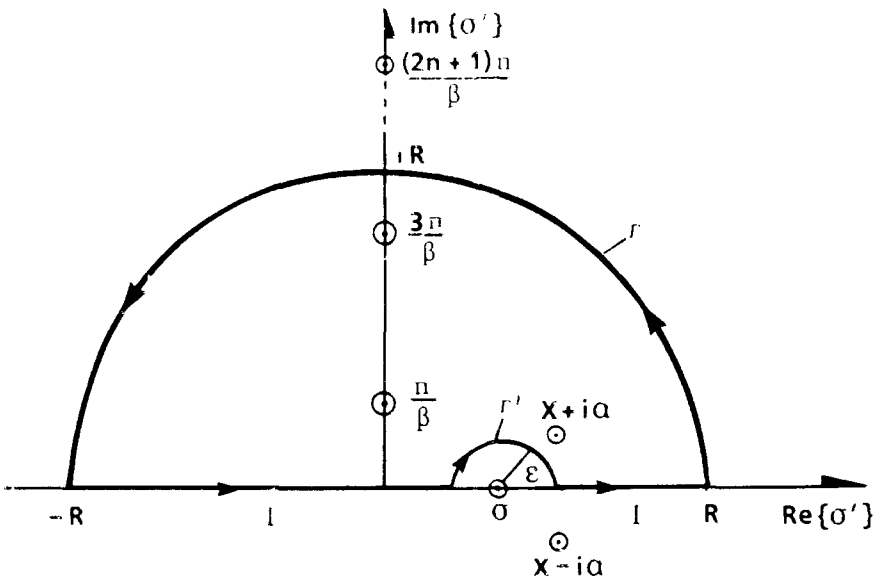

Figure 4.1 The integration contour C in the complex plane which is used in the evaluation of the integral in Equation (4.1) The poles of the integrand of Equation (4.1) are indicated by the symbol ⊙

The curve Γ in Figure 4.1 is a semicircle in the upper halfplane with radius R. It meets with the real axes at the points $\sigma' = -R$ and $\sigma' = R$, and it intersects the imaginary axes at the point $\sigma' = iR$. In appendix A it will be shown that the integrand of Equation (4.1) has infinitely many poles on the imaginary axes. There is, however, a finite distance unequal zero between these poles. This means that the curve Γ can always be made to intersect between two such poles.[2] In the limit where $R \to \infty$ the integral along the curve Γ will tend to zero since the integrand of Equation (4.2) goes to zero as R^{-3} for big $|\sigma'|$.

The curve Γ' is a small semicircle with radius ϵ centred in $\sigma' = \sigma$. The integral along this curve will be evaluated for the limit $\epsilon \to 0$ in Appendix A.

The curve I consists of two intervals on the real axis, namely $-R \leq \sigma' \leq \sigma - \epsilon$ and $\sigma + \epsilon \leq \sigma' \leq R$, where $\epsilon > 0$. In the limit $R \to \infty$ and $\epsilon \to 0$ the inte-

[2]This may of course slightly distort the value of the intergrand on the semicircle Γ, but in the limit $R \to \infty$ such a distortion will not change the value of the integral along Γ.

gral along I is the principal part of the integral in Equation (4.1). By means of the residue theorem the closed contour integral is given by

$$\int_C F(\sigma')d\sigma' = \int_I F(\sigma')d\sigma' + \int_\Gamma F(\sigma')d\sigma' + \int_{\Gamma'} F(\sigma')d\sigma' = 2\pi i \left[\begin{array}{l}\text{The sum of the residues of} \\ F(\sigma') \text{ inside the contour C}\end{array}\right] \tag{4.3}$$

In the limit $R\to\infty$ and $\epsilon\to 0$ the result is

$$PP\int_{-\infty}^{+\infty} F(\sigma')d\sigma' = 2\pi i \left[\begin{array}{l}\text{The sum of the residues of} \\ F(\sigma') \text{ inside the contour C}\end{array}\right] - \lim_{\epsilon\to 0}\int_{\Gamma'} F(\sigma')d\sigma \tag{4.4}$$

A detailed calculation of the right hand side of Equation (4.4) is described in Appendix A, and the result is given in Equation (A.18).

The result for the Hilbert transform described by Equation (4.1) is

$$F_\ell(\sigma,x) \equiv \frac{1}{\pi} PP\int_{-\infty}^{+\infty} F(\sigma')d\sigma' =$$

$$\frac{1}{\pi}\frac{x-\sigma}{(x-\sigma)^2+\alpha^2}\left[\frac{\sinh(\beta x)}{\cosh(\beta x)+\cos(\beta\alpha)} + \frac{1}{\pi}\,\mathrm{Im}\left\{\psi(\tfrac{1}{2}+i\frac{\beta}{2\pi}(x-i\alpha))-\psi(\tfrac{1}{2}+i\frac{\beta}{2\pi}(x+i\alpha))\right\}\right]$$

$$+\frac{1}{\pi}\frac{\alpha}{(x-\sigma)^2+\alpha^2}\left[\frac{\sin(\beta\alpha)}{\cosh(\beta x)+\cos(\beta\alpha)} + \frac{1}{\pi}\,\mathrm{Re}\left\{\psi(\tfrac{1}{2}+i\frac{\beta}{2\pi}(x-i\alpha))+\psi(\tfrac{1}{2}+i\frac{\beta}{2\pi}(x+i\alpha))\right\}\right.$$

$$\left. - \frac{2}{\pi}\,\mathrm{Re}\left\{\psi(\tfrac{1}{2}+i\frac{\beta}{2\pi}\sigma)\right\}\right] \tag{4.5}$$

The function $\psi(z)$ is the digamma function defined by

$$\psi(z) = \frac{d}{dz}(\ln\Gamma(z)) = \frac{\Gamma'(z)}{\Gamma(z)} \tag{4.6}$$

where $\Gamma(z)$ is the gamma function (9).

The Voigt dispersion function $F_V(\sigma,\sigma_j)$ defined in Equation (3.19) can

now be rewritten by Equation (4.5)

$$F_V(\sigma,\sigma_i) = \sqrt{\frac{\ln 2}{\pi}} \cdot \frac{1}{\alpha_d} \int_{-\infty}^{+\infty} F_\ell(\sigma,x) \cdot \exp\left[-\ln 2\left(\frac{x-\sigma_i}{\alpha_d}\right)^2\right]dx \qquad (4.7)$$

A notation equivalent to the one used in Equation (3.9) gives the following compact formula for the Voigt dispersion function

$$F_V(\sigma,\sigma_i) = \int_{-\infty}^{+\infty} F_\ell(\sigma,x) \cdot f_d(x,\sigma_i)dx \qquad (4.8)$$

where $f_d(\cdot,\cdot)$ is the Doppler line shape function.

The high pressure limit for the Voigt dispersion function is found from Equation (4.8) and (3.10)

$$\lim_{\alpha_d \to 0} F_V(\sigma,\sigma_i) = F_\ell(\sigma,\sigma_i) \qquad (4.9)$$

The Lorentz dispersion function, $F_\ell(\sigma,\sigma_i)$, is given by Equation (4.5) when the variable x is substituted with the resonance wave number, σ_i.

The low pressure limit for the Voigt dispersion function is also found from Equation (4.8) when the limit of Equation (4.5), as the Lorentz half width, α, tends to zero, is determined. The limit of Equation (4.5) is

$$\lim_{\alpha \to 0} F_\ell(\sigma,x) = \frac{1}{\pi}\frac{1}{x-\sigma} \cdot \tanh\left(\frac{\beta x}{2}\right) + \frac{2}{\pi}\delta(x-\sigma) \cdot \mathrm{Re}\left\{\psi\left(\frac{1}{2} + i\frac{\beta}{2\pi}x\right) - \psi\left(\frac{1}{2} + i\frac{\beta}{2\pi}\sigma\right)\right\} \qquad (4.10)$$

The low pressure limit for the Voigt dispersion function is then

$$\lim_{\alpha \to 0} F_V(\sigma,\sigma_i) = \frac{1}{\pi} \int_{-\infty}^{+\infty} \frac{1}{x-\sigma} \tanh\left(\frac{\beta x}{2}\right) f_d(x,\sigma_i)dx \qquad (4.11)$$

Since the integrand in (4.11) diverges where $x=\sigma$ the integration must

be performed by calculation of the principal part. In this respect Equation (4.11) is identical to Equation (3.22) defining the Doppler dispersion function, v.i.z

$$\lim_{a\to 0} F_v(\sigma,\sigma_i) = F_d(\sigma,\sigma_i) \tag{4.12}$$

An explicit expression for the Doppler dispersion function will not be calcualted in this report.

At this stage it is useful to remind oneself that the dispersion, $\Delta n(\sigma)$, given by Equation (3.15) has the following form

$$\Delta n(\sigma) = \frac{1}{4\pi} \sum_{ij} W(m_j)\tilde{S}_i(T)[F_v(\sigma,\sigma_i) + F_v(\sigma,-\sigma_i)] \tag{4.13}$$

By using Equations (4.5) and (4.9) it is now possible to give an explicit expression for the dispersion in the high pressure limit

$$\Delta n(\sigma) = \frac{1}{4\pi} \sum_{ij} W(m_j)\ \tilde{S}_i(T) \left[\frac{1}{\pi} \frac{\sigma_i - \sigma}{(\sigma_i-\sigma)^2 + a^2} \cdot T_1(\sigma_i) + \frac{1}{\pi} \frac{a}{(\sigma_i-\sigma)^2+a^2} \cdot T_2(\sigma,\sigma_i) \right.$$
$$\left. + \frac{1}{\pi} \frac{\sigma_i+\sigma}{(\sigma_i+\sigma)^2+a^2} \cdot T_1(\sigma_i) + \frac{1}{\pi} \frac{a}{(\sigma_i+\sigma)^2+a^2} \cdot T_2(\sigma,\sigma_i) \right] \tag{4.14}$$

The functions $T_1(\cdot)$ and $T_2(\cdot,\cdot)$ are easily identified from Equation (4.5). To establish Equation (4.14) the following relations are used

$$\begin{aligned} T_1(-\sigma_i) &= -T_1(\sigma_i) \\ T_2(\sigma,-\sigma_i) &= T_2(\sigma,\sigma_i) \end{aligned} \tag{4.15}$$

The well known anomalous dispersion form due to a resonance transition is recognized from the first term in Equation (4.14).

To illustrate the wave number dependence of the different terms in Equation (4.14) the four terms (exclusive the T_1 and T_2 functions) are plotted separately for two different resonance wave numbers (σ_i = 1 cm^{-1} and σ_i = 100 cm^{-1}) in the Figures 4.2 and 4.3. The Lorentz half width and the temperature are 0.1 cm^{-1} and 296 K. The

value of the functions $T_1(\sigma_1)$ and $T_2(\sigma,\sigma_i)_{\sigma=\sigma_i}$ is given (on the figures) for each resonance wave number.

Figure 4.2 illustrates the situation when the resonance wave number is 1 cm^{-1} The numbers refering to the different curves indicate the term number in Equation (4.14).

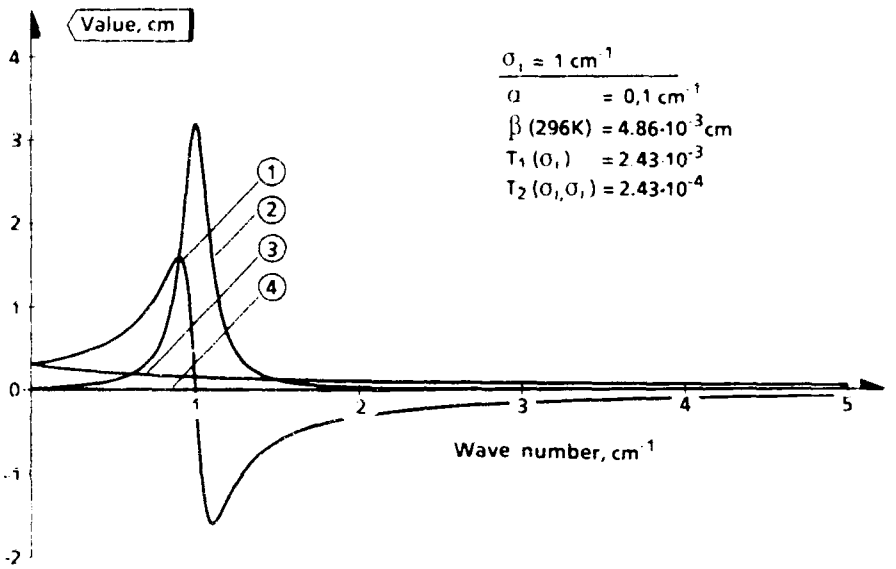

Figure 4.2 Wave number dependence of the different terms in Equation (4.14) for resonance wave number σ_i = 1 cm^{-1}
The functions $T_1(\sigma_i)$ and $T_2(\sigma,\sigma_i)_{\sigma=\sigma_i}$ have the values indicated

For the discussion of the results in Figure 4.2 the following symbolic representation of the wave number dependent part of Equation (4.14) is useful (Assuming $T_2(\sigma,\sigma_i)$ is a slowly varying function when $\sigma \approx \sigma_i$)

$$[\cdot] = ① \cdot T_1(\sigma_i) + ② \cdot T_2(\sigma_i,\sigma_i) + ③ \cdot T_1(\sigma_i) + ④ \cdot T_2(\sigma_i,\sigma_i) \tag{4.16}$$

The results in Figure 4.2 shows that the peak value of the first term in Equation (4.16) is dominating. The peak values of the second and third term are about one and two orders of magnitude less than the first term. The value of the fourth term is negligible.

At this point some comments about the values of the functions $T_1(\sigma_i)$

and $T_2(\sigma_i,\sigma_i)$ given in Figure 4.2 are worthwhile. Disregarding the diagamma function (this approximation is discussed in Chapter 5) these functions are given by:

$$T_1(\sigma_i) \approx \frac{\sinh(\beta\sigma_i)}{\cosh(\beta\sigma_i)+\cos(\beta\alpha)} \sim \tanh(\frac{\beta\sigma_i}{2}) \sim \frac{\beta\sigma_i}{2} \qquad (4.17)$$

$$T_2(\sigma,\sigma_i) \approx \frac{\sin(\beta\alpha)}{\cosh(\beta\sigma_i)+\cos(\beta\alpha)} \sim \frac{\beta\alpha}{\cosh(\beta\sigma_i)+1} \sim \frac{\beta\alpha}{2} \qquad (4.18)$$

when $\beta\alpha << 1$ and $\beta\sigma_i << 1$.

The values of $T_1(\sigma_i)$ and $T_2(\sigma_i,\sigma_i)$ given in Figure 4.2 are exactly reproduced by the approximations (4.17) and (4.18). The very low value of $T_1(\sigma_i)$ ($=2.43\cdot10^{-3}$) indicates that at this low resonance wave number stimulated emission is an important process with regard to dispersion (and absorption).

Figure 4.3 illustrates the situation when the resonance wave number is 100 cm^{-1}.

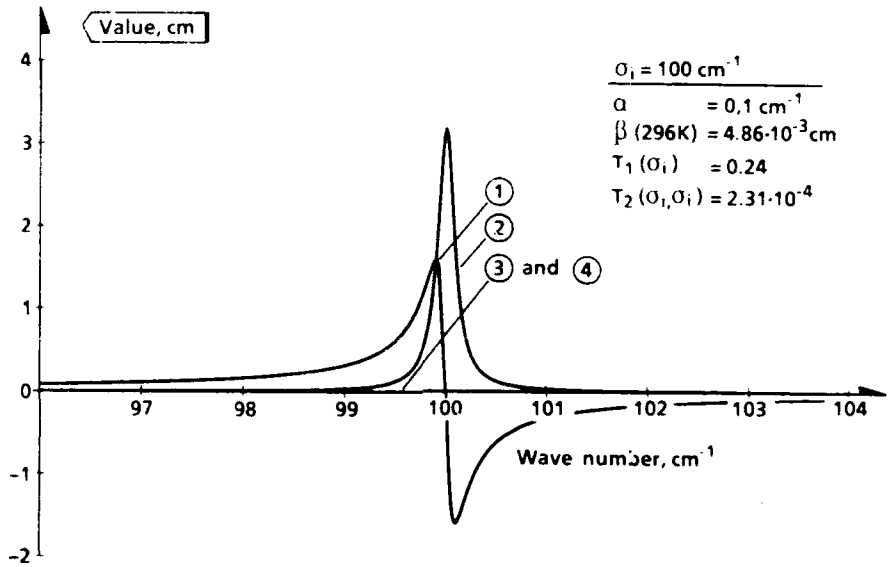

Figure 4.3 Wave number dependence of the different terms in Equation (4.14) for resonance wave number σ_i = 100 cm^{-1}
The functions $T_1(\sigma_i)$ and $T_2(\sigma,\sigma_i)_{\sigma=\sigma_i}$ have the values indicated

The results in Figure 4.3 shows that the peak value of the first term in Equation (4.16) is dominating with at least two orders of magnitude over the other terms.

The values of $T_1(\sigma_i)$ and $T_2(\sigma_i,\sigma_i)$ stated in Figure 4.3 are almost exactly reproduced by the approximations (4.17) and (4.18). The value of $T_1(\sigma_i)$ (0.24) has increased by two orders of magnitude indicating the reduced importance of stimulated emission as the resonance wave number increases.

The part of the approximations in (4.17) and (4.18) which are valid when only $\beta\sigma \ll 1$ shows that $T_1(\sigma_i) \to 1$ and $T_2(\sigma,\sigma_i) \to 0$ when the resonance wave number increases. For $\sigma_i > 500$ cm^{-1}, $T_1(\sigma_i) > 0.84$ and $T_2(\sigma,\sigma_i) < 8.5\cdot10^{-5}$ when the temperature is 296 K.

As a result of this discussion it is reasonable to assume that, at standard atmospheric pressure (Lorentz broadning dominates) and temperature, the dispersion in the infrared and visible part of the spectrum is well approximated by

$$\Delta n(\sigma) = \frac{1}{4\pi^2} \sum_{ij} W(m_j) \cdot \tilde{S}_i(T) \cdot \frac{\sigma_i-\sigma}{(\sigma_i-\sigma)^2+\alpha^2} \qquad (4.19)$$

The result in Equation (4.19) could easily be obtained by doing the following approximations in the expression for the optical depth (Equation (3.1)) $\tanh(\beta\sigma/2) = 1$ and $f(-\sigma,\sigma_i) = 0$ prior to the Hilbert transformation.

A general line by line calculation of the dispersion valid for different pressures and temperatures may in principle be implemented by means of the Equations (4.5), (4.7) and (4.13). However, the presence of the digamma function in Equation (4.5) makes such an implementation rather awkward. In the next chapter approximations that simplify the expression of Equations (4.5) and (4.7) will be made. The validity of these approximations in different domains of wave numbers and thermodynamic parameters will be discussed. One of these approximations will be implemented as a computer program for line by line calculation.

(cm²/molecule)

5 APPROXIMATIONS AND IMPLEMENTATION IN FASCOD2

The aim of the work described in this chapter is to develop an approximation for the dispersion formulas calculated in Chapter 3 which is suitable for line by line calculation within the framework of FASCOD2 (10).

The first part of this chapter will mainly discuss the importance of the different terms in the dispersion formulas especially the Lorentz dispersion function given by Equations (4.9) and (4.5). The result of this discussion will establish certain domains for the resonance wave numbers and the thermodynamic parameters where different approximations for the Lorentz dispersion function are valid.

The second part of this chapter describes one specific approximation and the implementation of this approximation in FASCOD2 for line by line calculation of dispersion.

5.1 Approximations for the Lorentz dispersion function

The discussion in this part will concentrate on approximations for the Lorentz dispersion function, $F_\ell(\sigma,\sigma_i)$, given by Equation (4.9) and (4.5). The reason is that a valid approximation for the Lorentz dispersion function also imply a valid approximation for the Voigt dispersion function given by

$$F_v(\sigma,\sigma_i) = \sqrt{\frac{\ln 2}{\pi}} \cdot \frac{1}{\alpha_d} \int_{-\infty}^{+\infty} F_\ell(\sigma,x) \cdot \exp[-\ln 2 \, (\frac{x-\sigma_i}{\alpha_d})^2]dx \qquad (5.1)$$

This statement requires that the exponential in Equation (5.1) has diminishing values near the edge of the validity region for the approximate Lorentz dispersion function. In other words the validity region for the approximate Voigt dispersion function will be some Doppler half widths less than the validity region for the approximate Lorentz dispersion function.

From Equation (4.5), (4.9) and (4.14) the complete expressions for the Lorentz dispersion functions are

$$F_\ell(\sigma,\sigma_i) = \frac{1}{\pi}\frac{\sigma_i-\sigma}{(\sigma_i-\sigma)^2+\alpha^2}\cdot T_1(\sigma_i) + \frac{1}{\pi}\cdot\frac{\alpha}{(\sigma_i-\sigma)^2+\sigma^2}\cdot T_2(\sigma,\sigma_i)$$

$$F_\ell(\sigma,-\sigma_i) = \frac{1}{\pi}\frac{\sigma_i+\sigma}{(\sigma_i+\sigma)^2+\alpha^2}\cdot T_1(\sigma_i) + \frac{1}{\pi}\cdot\frac{\alpha}{(\sigma_i+\sigma)^2+\sigma^2}\cdot T_2(\sigma,\sigma_i) \qquad (5.2)$$

where

$$T_1(\sigma_i) = \frac{\sinh(\beta\sigma_i)}{\cosh(\beta\sigma_i)+\cos(\beta\alpha)} + \frac{1}{\pi}\mathrm{Im}\left\{\psi(\tfrac{1}{2}+\frac{i\beta}{2\pi}(\sigma_i-i\alpha)) - \psi(\tfrac{1}{2}+\frac{i\beta}{2\pi}(\sigma_i+i\alpha))\right\} \qquad (5.3)$$

$$T_2(\sigma,\sigma_i) = \frac{\sin(\beta\alpha)}{\cosh(\beta\sigma_i)+\cos(\beta\alpha)} + \frac{1}{\pi}\mathrm{Re}\left\{\psi(\tfrac{1}{2}+\frac{i\beta}{2\pi}(\sigma_i-i\alpha)) + \psi(\tfrac{1}{2}+\frac{i\beta}{2\pi}(\sigma_i+i\alpha))\right\}$$

$$- \frac{2}{\pi}\mathrm{Re}\left\{\psi(\tfrac{1}{2}+\frac{i\beta}{2\pi}\sigma)\right\}$$

In order to do a line by line computation of dispersion based on the Voigt dispersion function, Equation (5.1), or even the Lorentz dispersion function, the functions $T_1(\sigma_i)$ and $T_2(\sigma,\sigma_i)$ are rather awkward. Especially the digamma functions with complex arguments.

It is therefore necessary to analyse the value of the terms in Equation (5.3) in order to determine a domain of resonance wave numbers and thermodynamic parameters where the digamma functions can be neglected. This analysis is described in detail in Appendix B. The result is given in Equation (B.10) stating that the diagamma functions can be neglected when

$$\frac{\sinh(\beta\sigma_i)}{\cosh(\beta\sigma_i)+\cos(\beta\alpha)} \gg \frac{3}{\pi^2}\,\beta\alpha \qquad (5.4)$$

Since the value of $\beta\cdot\alpha$ ($= hc/kT\cdot\alpha$) normally is much less than one (in atmospheric physics $\beta\cdot\alpha < 10^{-2}$) the inequality (5.4) is equivalent to

$$\sigma_i \gg \frac{2}{\beta} \operatorname{arctanh}\left(\frac{3}{\pi^2}\beta\alpha\right) \approx \frac{6}{\pi^2}\alpha \tag{5.5}$$

In atmospheric physics the maximum value of the Lorentz half width is of the order 0,5 cm^{-1}. A neglection of the digamma functions is then a valid approximation when

$$\sigma_i \gg 0{,}3\ cm^{-1} \tag{5.6}$$

This means that the digamma functions have some influence on atmospheric dispersion for resonance transitions in the wavenumber interval up to ~1 cm^{-1}. In the visible and infrared wave number domain the influence of these functions are of no importance, but atmospheric influence on electromagnetic radiation with wave number less than 1 cm^{-1} (corresponding to a frequency of 30 GHz) is of great importance in many technological applications.

When the inequality (5.4) holds it is possible to define approximate Voigt and Lorentz dispersion functions, $F_{vA}(\sigma,\sigma_i)$ and $F_{\ell A}(\sigma,\sigma_i)$

$$F_{vA}(\sigma,\sigma_i) = \int_{-\infty}^{+\infty} F_{\ell A}(\sigma,x)\cdot f_d(x,\sigma_i)dx \tag{5.7}$$

where

$f_d(x,\sigma_i)$ - The Doppler line shape function

$$F_{\ell A}(\sigma,\sigma_i) = \frac{1}{\pi}\frac{\sigma_i-\sigma}{(\sigma_i-\sigma)^2+\alpha^2}\cdot T_{1A}(\sigma_i) + \frac{1}{\pi}\frac{\alpha}{(\sigma_i-\sigma)^2+\alpha^2} T_{2A}(\sigma_i) \tag{5.8}$$

$$T_{1A}(\sigma_i) = \frac{\sinh(\beta\sigma_i)}{\cosh(\beta\sigma_i)+\cos(\beta\alpha)} \tag{5.9}$$

$$T_{2A}(\sigma_i) = \frac{\sin(\beta\alpha)}{\cosh(\beta\sigma_i)+\cos(\beta\alpha)}$$

In order to get a picture of the importance of the different terms and

variables in the approximate Voigt dispersion function a computer program that performs the integration in Equation (5.7) for one single resonance transition is developed. In this case the dispersion is given by the simplified formula

$$\Delta n(\sigma) = \frac{1}{4\pi} W(m_i) \tilde{S}_i [F_{vA}(\sigma,\sigma_i) + F_{vA}(\sigma,-\sigma_i)] \qquad (5.10)$$

The programme calculates only the sum of the two approximate Voigt dispersion functions in Equation (5.10). This sum can be expressed as a sum of a Dominating term, $F_{vAD}(\sigma,\sigma_i)$, and a Correcting term, $F_{vAC}(\sigma,\sigma_i)$, v.i.z

$$F_{vA}(\sigma,\sigma_i) + F_{vA}(\sigma,-\sigma_i) = F_{vAD}(\sigma,\sigma_i) + F_{vAC}(\sigma,\sigma_i) \qquad (5.11)$$

where

$$F_{vAD}(\sigma,\sigma_i) = \int_{-\infty}^{+\infty} T_{1A}(x) \frac{1}{\pi} \frac{x-\sigma}{(x-\sigma)^2+\alpha^2} f_d(x,\sigma_i)dx \qquad (5.12)$$

$$F_{vAC}(\sigma,\sigma_i) = \int_{-\infty}^{+\infty} T_{1A}(x) \frac{1}{\pi} \frac{x+\sigma}{(x+\sigma)^2+\alpha^2} f_d(x,\sigma_i)dx$$

$$+\int_{-\infty}^{+\infty} T_{2A}(x) \left\{ \frac{1}{\pi} \frac{\alpha}{(x-\sigma)^2+\sigma^2} + \frac{1}{\pi} \frac{\alpha}{(x+\sigma)^2+\alpha^2} \right\} f_d(x,\sigma_i)\, dx \qquad (5.13)$$

$$f_d(x,\sigma_i) = \sqrt{\frac{\ln 2}{\pi}} \cdot \frac{1}{\alpha_d} \exp[-\ln 2 \, (\frac{x-\sigma_i}{\alpha_d})^2] \qquad (5.14)$$

The calculation of the sum in Equation (5.11) and the correcting term in Equation (5.13) is done for two different thermodynamic situation. One in the high pressure limit where the homogeneous (Lorentz) broadening dominates and one in the intermediate regime where the homogeneous and inhomogeneous (Doppler) line widths are equal. The calculations are done for two resonance wave numbers $\sigma_i = 1$ cm^{-1} and $\sigma_i = 100$ cm^{-1}. The Doppler line width used in the calculations is adequate for a H_2O molecule.

The Figures 5.1 and 5.2 show both the sum of the dominating and correcting term and the correcting term only for the two different thermodynamic situations when the resonance wave number is 1 cm^{-1}.

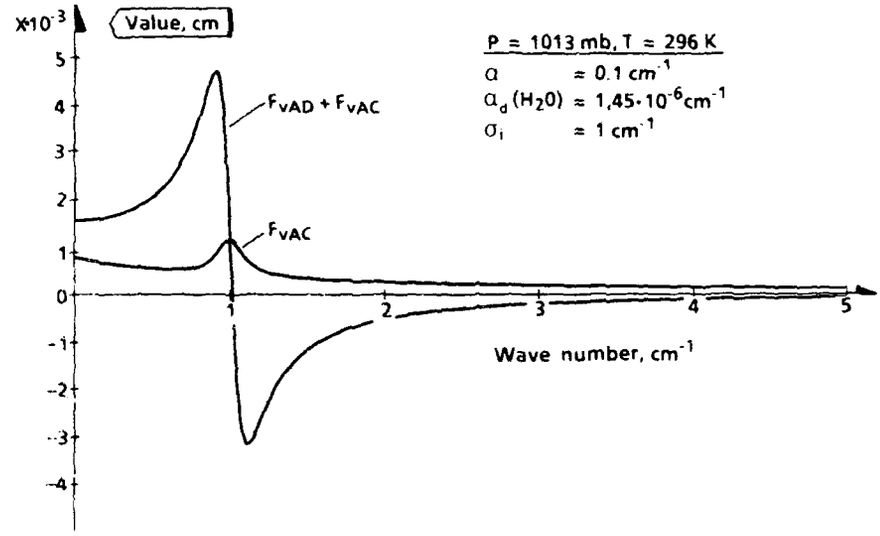

Figure 5.1 The total Voigt dispersion function (5.11) and the correcting term (5.12) at standard temperature and pressure when $\sigma_i = 1\ cm^{-1}$
($\beta = 4.86 \cdot 10^{-3}$ cm, $T_{1A}(\sigma_i) = 2{,}43 \cdot 10^{-3}$, $T_{2A}(\sigma_i) = 2.43 \cdot 10^{-8}$)

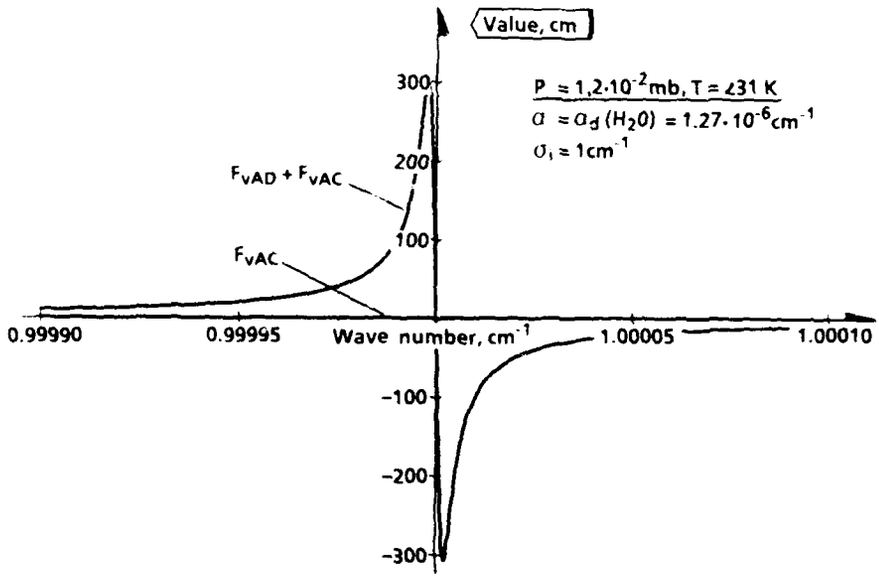

Figure 5.2 The total Voigt dispersion function (5.11) and the correcting term (5.12) when the Lorentz and Doppler half widths are equal and $\sigma_i = 1\ cm^{-1}$
($\beta = 6.23 \cdot 10^{-3}$ cm, $T_{1A}(\sigma_i) = 3{,}11 \cdot 10^{-3}$, $T_{2A}(\sigma_i) = 3.96 \cdot 10^{-8}$)

The big differences between the shapes and peak values in Figure 5.1 and 5.2 are mainly due to the five order of magnitude change of the effective line width. This is also the reason for the vanishing correcting term in Figure 5.2. When the results in Figure 5.1 and 5.2 are used for calculation of the dispersion by Equation (5.10) (assuming equal line strength $\tilde{S}_i$) the number density must be scaled properly by the factor $(p/p_0)\cdot(T_0/T))$. The resulting peak dispersion is almost equal for the two situations.

Figure 5.3 and 5.4 show almost the same situations as the preceeding figures when the resonance wave number is 100 cm^{-1}.

The difference in shape and peak values between Figure 5.3 and 5.4 is mainly due to the tree order of magnitude change of the effective line width. The correcting term vanishes in both situations mainly because the resonance wave number is increased by two orders of magnitude. The peak value in Figure 5.4 scaled by the number density factor is almost equal to the peak value in Figure 5.3 resulting in about equal peak dispersion for the two situations (assuming equal line strength $\tilde{S}_i$).

The peak value of the dispersion for resonance wave number 100 cm^{-1} is however about two orders of magnitude greater than the peak value of the dispersion for resonance wave number 1 cm^{-1}. This is seen by comparing the peak values in Figure 5.1 and 5.3. (The same result is obtained by comparing the peak values of Figure 5.2 and 5.4 after proper scaleing by the number density factor). The reason is that the value of the function $T_{1A}(\sigma_i)$ is almost linear with wave number in this region. This again demonstrates the reduced importance of stimulated emission with increasing resonance wave number.

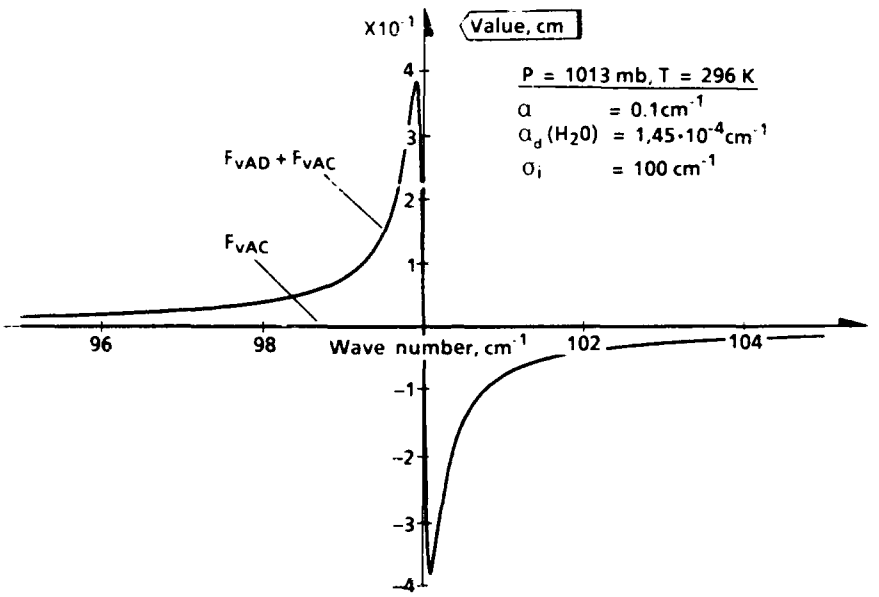

Figure 5.3 The total Voigt dispersion function (5.11) and the correcting term (5.12) at standard temperature and pressure when $\sigma_i = 100\ cm^{-1}$ ($\beta = 4.86 \cdot 10^{-3}$ cm, $T_{1A}(\sigma_i) = 0.24$, $T_{2A}(\sigma_i) = 2.31 \cdot 10^{-4}$)

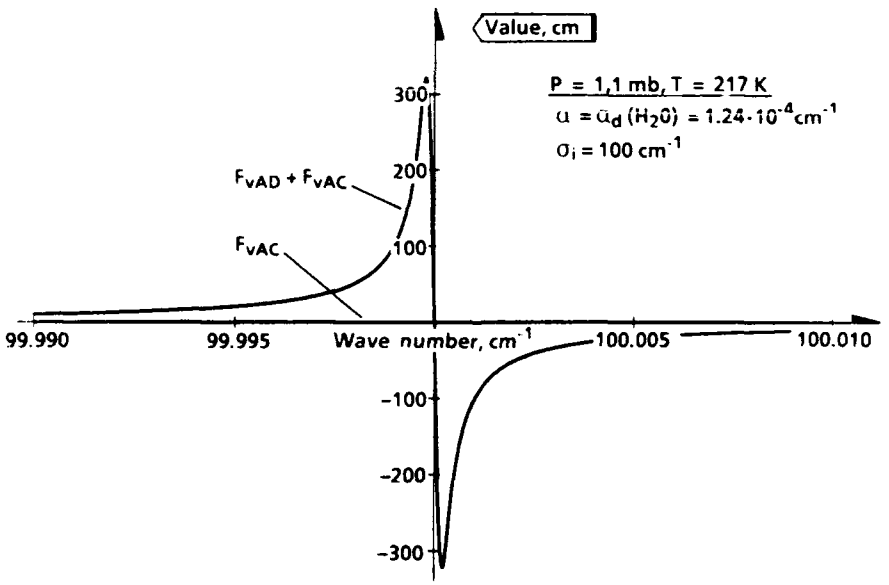

Figure 5.4 The total Voigt dispersion function (5.11) and the correcting term (5.12) when the Lorentz and Doppler half widths are equal and $\sigma_i = 100\ cm^{-1}$ ($\beta = 6.63 \cdot 10^{-3}$ cm, $T_{1A}(\sigma_i) = 0,33$, $T_{2A}(\sigma_i) = 8.22 \cdot 10^{-7}$)

5.2 Implementation in FASCOD2

The discussion in this part will concentrate on the implementation of an appropriate formula for line by line computation of dispersion by a slightly modified FASCOD2.

For line by line computation of absorbtion the Voigt line shape function of Equation (3.5) is used. This necessitates a numerical integration to achieve each value of the Voigt line shape. To speed up this integration process a special algorithm has been developed based on the fact that the Voigt line shape has a "fall off" $\sim (\sigma-\sigma_i)^{-2}$ distant from the line center while the inhomogenous (Doppler) broadning is important near the line center.

This algorithm will probably not give a correct result for the approximative Voigt dispersion function of Equation (5.7) since the dominating term has a "fall off" $\sim (\sigma-\sigma_i)^{-1}$ (see Equation (5.12)) distant from the line center. To implement the Voigt dispersion function in FASCOD2 a new algorithm for numerical integration has to be developed. This problem is not addressed in this report.

Due to the lack of a new numerical integration algortihm only the approximative Lorentz dispersion function has been implemented in FASCOD2. The implemented formula for line by line computation of dispersion is

$$\Delta n(\sigma) = \frac{1}{4\pi} \sum_{ij} W(m_j)\, \tilde{S}_i(T)\, [F_{\ell A}(\sigma,\sigma_i)+F_{\ell A}(\sigma,-\sigma_i)] \tag{5.15}$$

where

$$F_{\ell A}(\sigma,\sigma_i) = \frac{1}{\pi} \frac{\sigma_i-\sigma}{(\sigma_i-\sigma)^2+\alpha^2}\, T_{1A}(\sigma_i)+\frac{1}{\pi} \frac{\alpha}{(\sigma_i-\sigma)^2+\alpha^2}\, T_{2A}(\sigma_i) \tag{5.16}$$

$$F_{\ell A}(\sigma,-\sigma_i) = \frac{1}{\pi} \frac{\sigma_i+\sigma}{(\sigma_i+\sigma)^2+\alpha^2}\, T_{1A}(\sigma_i)+\frac{1}{\pi} \frac{\alpha}{(\sigma_i+\sigma)^2+\alpha^2}\, T_{2A}(\sigma_i) \tag{5.17}$$

$$T_{1A}(\sigma_i) = \frac{\sinh(\beta\sigma_i)}{\cosh(\beta\sigma_i)+\cos(\beta\alpha)} \tag{5.18}$$

$$T_{2A}(\sigma_i) = \frac{\sin(\beta\alpha)}{\cosh(\beta\sigma_i)+\cos(\beta\alpha)} \tag{5.19}$$

$\beta = hc/kT$

α - Lorentz half width (HWHM); function of temperature and pressure

The connection between the line strength, $\tilde{S}_i(T)$, in Equation (5.15) and the line strength, $S_i(T)$, filed on the HITRAN molecular database (11) is

$$\tilde{S}_i(T) = \frac{S_i(T)}{\sigma_i \tanh(\frac{\beta\sigma_i}{2})} \tag{5.20}$$

The units of the HITRAN line strength is cm/molecule.

Equation (5.15) should give an adequate description of the dispersion in a mixture of gases when the following conditions are fulfilled:

a) The dipole approximation and a classical description of the radiation field are valid

b) Line coupling effects are negligible

c) Homogenous (Lorentz) broadning is dominant

d) The resonance wave number $\sigma_i \geq 1$ cm^{-1}

The theoretical description in this report makes it possible to defeat condition d) by introducing the digamma functions in Equations (5.18) and (5.19), and condition c) by developing a new numerical integration algorithm for the Voigt dispersion function.

6 LINE BY LINE CALCULATION OF ATMOSPHERIC DISPERSION

This chapter describes results from some line by line calculations of atmospheric dispersion by FASCOD2 modified according to Equations (5.15)-(5.19). Four results are presented and discussed. These results show the atmospheric dispersion in different wave number regions at different spectral resolution for the Midlatitude summer model, i e temperature 294 K, pressure 1013 mb and a water content of 14 g/m^3 at ground level.

Figure 6.1 shows a result where the contribution to the dispersion steems mostly (though not totally), from one single transition in the water molecule with resonance wavenumber σ_i = 1684.837 cm^{-1} and Lorentz half width α = 0.0962 cm^{-1}.

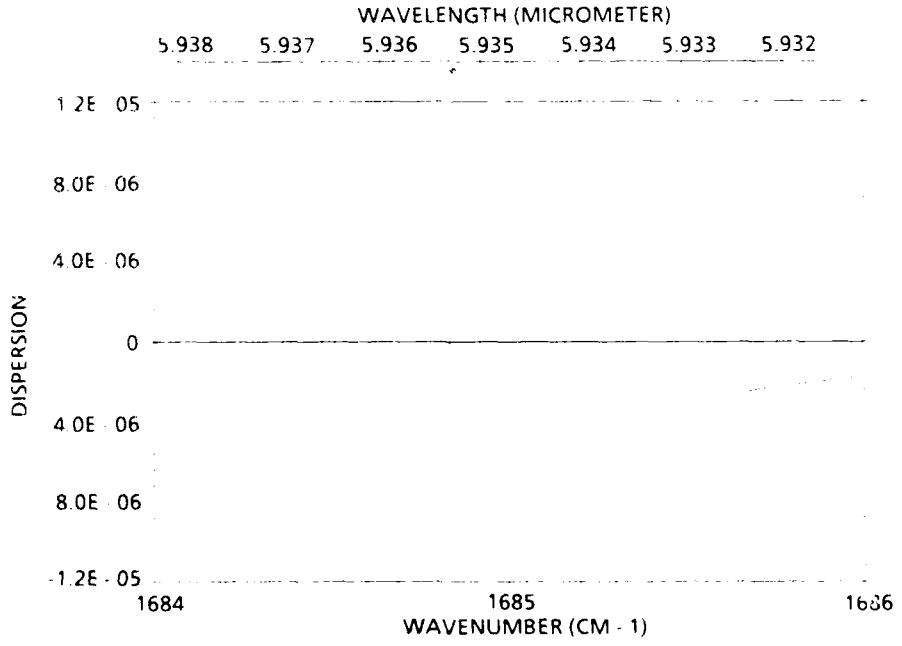

Figure 6.1 The atmospheric dispersion at ground level in the wave number interval 1684-1686 cm^{-1} for the Midlatitude summer model.
The main contribution to the dispersion is from a transition in the water molecule with resonance wavenumber σ_i = 1684.837 cm^{-1}.

The result in Figure 6.1 shows the classical dispersion connected to one single resonance transition. The maximum and minimum value of the dispersion in Figure 6.1 are

$$\Delta n_{max} = 8.9 \cdot 10^{-6} \tag{6.1}$$

$$\Delta n_{min} = -1.0 \cdot 10^{-5} \tag{6.2}$$

For this single line in the infrared part of the spectrum it is easy to verify the result in Figure 6.1 from Equation (4.19). For a single line Equation (4.19) is modified to read

$$\Delta n(\sigma) = \frac{1}{4\pi^2} \cdot W(m_i) \cdot \tilde{S}_i(T) \cdot \frac{\sigma_i - \sigma}{(\sigma_i - \sigma)^2 + \alpha^2} \tag{6.3}$$

By introducing the HITRAN line strength from Equation (5.20) and the approximation $\tanh(\beta\sigma_i/2) \approx 1$ in the infrared at standard temperature, Equation (6.3) is modified to

$$\Delta n(\sigma) = \frac{1}{4\pi^2} \cdot \frac{1}{\sigma_i} \cdot \frac{\sigma_i - \sigma}{(\sigma_i - \sigma)^2 + \alpha^2} \cdot W(m_i) \cdot S_i(T) \tag{6.4}$$

The maximum and minimum value of Equation (6.4) occur when the wave number is equal to $\sigma_i \pm \alpha$ and the peak values of the dispersion are

$$\Delta n_{max,min} = \pm \frac{1}{8\pi^2} \cdot \frac{W(m_i) \cdot S_i(T)}{\sigma_i \cdot \alpha} \tag{6.5}$$

when

$$\sigma_{max,min} = \sigma_i \pm \alpha \tag{6.6}$$

The number density of water molecules and the line strength on the HITRAN data base for this transition gives the following value for the product of number density and line strength

$$W(m_i) \cdot S_i(T) = 0.1304 \text{ cm}^{-2} \tag{6.7}$$

Wave number and value for the peak dispersion calculated from Equation (6.5) and (6.6) is

$$\Delta n_{max,min} = \pm 1.0 \cdot 10^{-5} \tag{6.8}$$

$$\sigma_{max} = 1684.741 \text{ cm}^{-1}$$

$$\sigma_{min} = 1684.933 \text{ cm}^{-1} \tag{6.9}$$

The calculated result in (6.8) and (6.9) are in very good agreement with the results presented in Figure 6.1. Wave number and value for the minimum dispersion have the best agreement due to less influence from another resonance line at lower wavenumbers in the FASCOD2 calculations.

The conclusion from the preceeding comparison between the FASCOD2 result and a theoretical result is that the implementation in FASCOD2 most probably performs a correct calculation of the dispersion.

Figure 6.2 shows the atmospheric dispersion in the wavenumber region 35-45 cm^{-1}, where several transitions in the water molecule are contributing to a rather complex result due to interference between different lines. The atmospheric model is still Midlatitude summer at ground level.

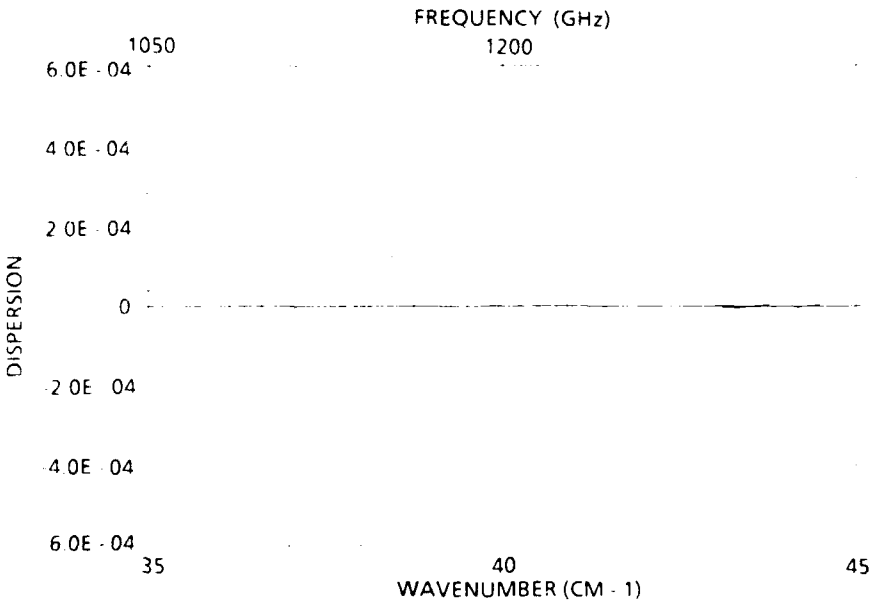

Figure 6.2 The atmospheric dispersion at ground level in the wave number interval 35-45 cm^{-1} for the Midlatitude summer model.
Several transitions in the water molecule with different line strength are contributing.

The complex nature of the dispersion in Figure 6.2 is due to the interference between a number of different water vapour lines with different line strength. The peak dispersion in Figure 6.2 is about one order of magnitude greater than the peak dispersion in Figure 6.1. This effect can be infered from Equation (6.5) although this equation is not strictly correct in this wavenumber region.

Figure 6.3 shows the atmospheric dispersion for the entire wavenumber region 0-500 cm^{-1}. The majority of the "lines" are due to transitions in the water molecule.

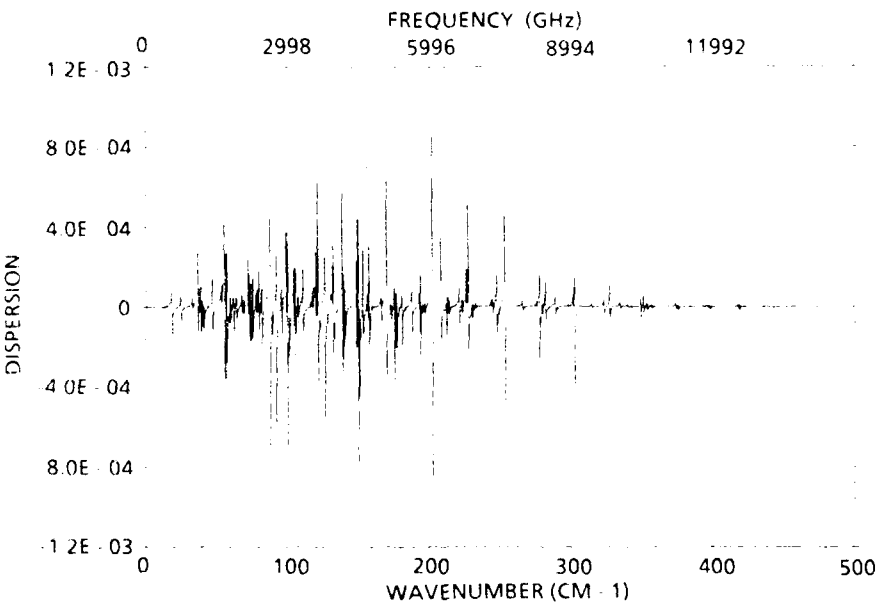

Figure 6.3 Atmospheric dispersion at ground level in the wavenumber interval 0-500 cm^{-1} for the Midlatitude summer model.
The main contribution to the dispersion steems from several transition in the water molecule

The maximum and minimum value of the dispersion in Figure 6.3 is $1.06 \cdot 10^{-3}$ for the resonance line near 150 cm^{-1}. By anticipating the validity of Edlén's formula, see (1), for dry air in the μ-wave region it is possible to calculate the maximum and minimum value of the refractive index around ~150 cm^{-1} for the gas mixture in this example. Edlén's formula corrected for a temperature of 294 K gives (σ = 150 cm^{-1}).

$$(n-1)_{dry} = 2.6 \cdot 10^{-4} \tag{6.10}$$

The influence of water vapour on the refractive index then gives the following maximum and minimum value for the refractive index of the gas mixture near the wave number 150 cm^{-1}

$$\begin{bmatrix} n_{max} \\ n_{min} \end{bmatrix} = 1 + 0.26 \cdot 10^{-3} \pm 1.06 \cdot 10^{-3} = \begin{bmatrix} 1.00132 \\ 0.99920 \end{bmatrix} \tag{6.11}$$

The calculations in (6.11) show the rather peculiar result that the minimum refractive index is less than unity. The calculations also show that every resonance line in Figure 6.3 with a minimum value for the dispersion less than $2.6 \cdot 10^{-4}$ will exhibit a corresponding minimum refractive index less than unity. The majority of the resonance lines in this wave number region will, as seen from Figure 6.3, exhibit this pecularity. Whether these results are correct remains to be determined by experiments.

Figure 6.4 shows the atmospheric dispersion in the wave number interval 2300-2400 cm^{-1} for the Midlatitude summer model, at ground level. It is mainly the CO_2 molecule that contributes to the dispersion in this wavenumber interval.

The structures of the dispersion in Figure 6.4 are due to the P- and R-branch of viberational-rotational transition of CO_2 centered at wave number 2349.146 cm^{-1}.

In this wave number interval the Edlén formula gives the following value for the refractive index of dry air (σ = 2350 cm^{-1})

$$(n-1)_{dry} = 2.7 \cdot 10^{-4} \tag{6.12}$$

The peak dispersion in Figure 6.4 are about two orders of magnitude less than the Edlén value. Resonance lines in this wave number region therefore contribute negligible to the refractive index of air in the Midlatitude summer model.

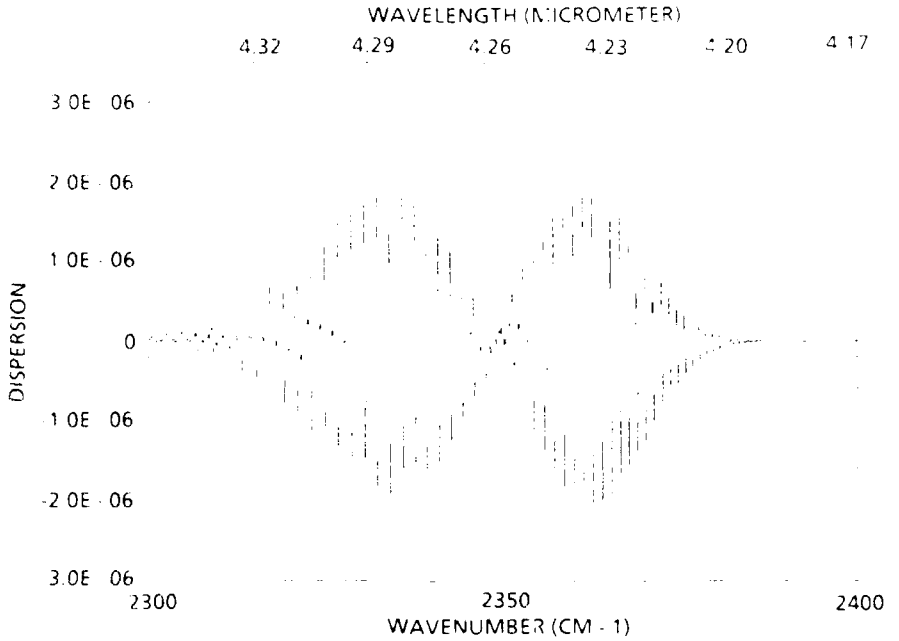

Figure 6.4 Atmospheric dispersion at ground level in the wave number interval 2300-2400 cm^{-1} for the Midlatitude summer model. It is mainly CO_2 that contributes to the disperison in this interval.

An overview of the dispersion for the entire wave number region 500 cm^{-1} - 15000 cm^{-1} for the Midlatitude summer model is given in Apperdix C.

The input data for FASCOD2 are as mentioned provided by the line data base HITRAN. This database contains line data for molecular transitions with resonance wave numbers in the wave number interval 0-17900 cm^{-1}. In the wave number interval above 5000 cm^{-1} the dispersion is a very small quantity in air (less than $3 \cdot 10^{-7}$ for the Midlatitude summer model). It has not been possible to find measurements with an accuracy that makes the verification of the fine structure of our computations possible in this interval. Below 5000 cm^{-1} there are wave number intervals where the dispersion has a substantially higher value. The most interesting domain, when it comes to comparisons between calculations and measurements, is the wave number interval 0-500 cm^{-1}. In this wave number interval the modified version of FASCOD2 predicts that the value of the disperison is in the range $\pm 1.2 \cdot 10^{-3}$ for the Midlatitude summer model.

A paper by Liebe, (3), investigates a model made for the computation of attenuation and dispersive delay in the wave number interval 0-33 cm^{-1}. Comparisons between his model and measurements are done, and Liebe claims that good agreement between model predictions and field/laboratory experiments is obtained.

Figure 6.5 shows the results from Liebe's model for the dispersion, whilst Figure 6.6 shows the dispersion calculated by the modified version of FASCOD2. The gas mixture and thermodynamic parameters are identical.

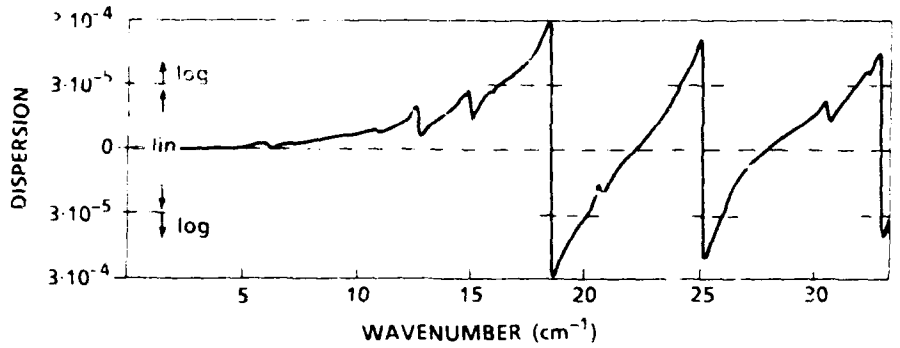

Figure 6.5 The calcualted dispersion for air where the relative humidity is 100%, the temperature is 303 K and the pressure is 1013 mb. From Liebe. (3).

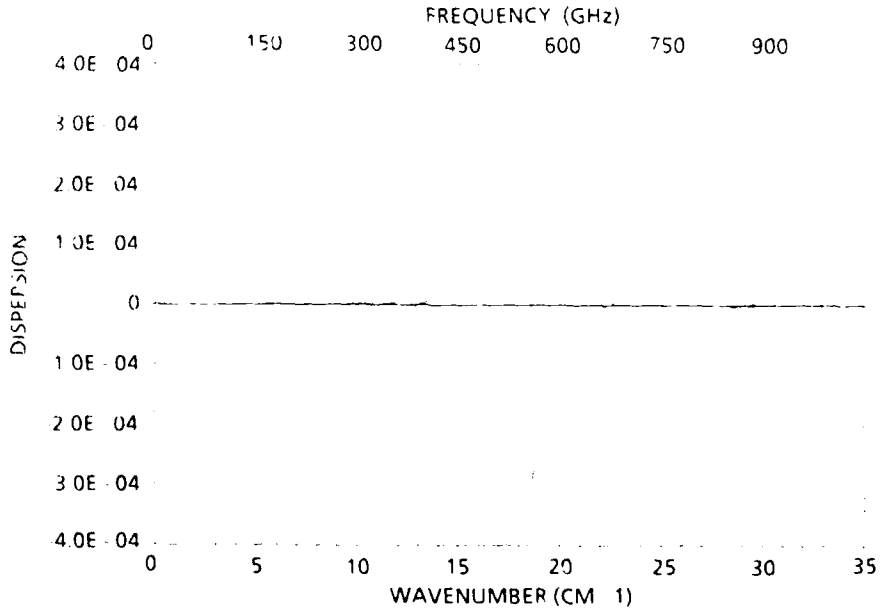

Figure 6.6 The dispersion calculated by the modified version of FASCOD2.
The gas mixture and the thermodynamic parameters are identical to those used by Liebe (3).

A close comparison between the dispersion in Figure 6.5 and 6.6 shows excellent agreement especially between the peak dispersion at 18.5 cm^{-1} wave number.

The results presented in this chapter demonstrate that the modified version of FASCOD2 performs a correct line by line calculation of the dispersion due to resonance transitions when homogenous (Lorentz) broadening is dominant.

7 CONCLUSIONS AND PROPOSITIONS FOR FURTHER RESEARCH

From the connection between the complex propagation constant of an electromagnetic field in a medium and the complex linear susceptibility, a Hilbert transform relationship between the anomalous dispersion and the optical depth has been established via the Kramer-Kronig relations. Based on the Van Vleck-Huber formalism for the optical depth an explicit expression for the dispersion in a mixture of gases is developed. This expression determines the dispersion whether the line shape is described by the Voigt, Lorentz or Doppler line shape functions.

The derived dispersion is valid for all wavenumbers provided the dipole approximation is valid and a classical description of the electromagnetic field is adequate. The effect of line coupling is not taken into account. The Hilbert transformation of the optical depth is performed without approximations.

The importance of the different terms in the derived expression is visualized and discussed by numerical examples.

Since the complete expression for the dispersion is rather awkward for numerical computations an approximation is developed. This approximate expression for the dispersion is valid when the resonance wave number for a transition is greater than 1 cm^{-1} (30 GHz). Numerical examples of the approximate dispersion for a single resonance line described by

a Voigt line shape function is also visualized and discussed.

In order to perform a line by line computation of the dispersion in a mixture of gases the computer code FASCOD2, developed by the US Air Force Geophysics Laboratory (AFGL), has been modified. The modified version of FASCOD2 only performs correct computation of the dispersion when the gas pressure is in the regime where homogenous (Lorentz) broadning is dominant and the resonance wave number is greater than 1 cm^{-1}.

Examples of line by line calculated atmospheric dispersion for the Midlatitude Summer model at standard atmospheric pressure are given. One example shows that the calculated dispersion from FASCOD2 is identical to the theoretical result for a specific transition in the infrared region. This result confirms that the modifications in FASCOD2 are correct. Another example from the wave number region 1-33 cm^{-1}, is a comparison between the calculated result from FASCOD2 and the measurements of H J Liebe at the Institute for Telecommunication Sciences, USA. These two results are in excellent agreement.

The result from these two examples leads to the conclusion that the theoretical expression for the dispersion derived in this report and the implementation in FASCOD2 gives a correct line by line computation of the dispersion in a mixture of gases when line coupling effects are negligible.

In order to achieve increased confidence in the theoretical results derived in this report a greater effort is needed. The rest of this chapter is therefore devoted to propositions for further research.

Results from the existing modified FASCOD2 should be compared with high resolution measurement of dispersion in different wavenumber regions at different temperature and humidity.

In order to do line by line calculations for resonance transitions < 1 cm^{-1} (30 GHz) the neglected digamma functions in the Lorentz dispersion function should be incorporated in the existing line by line code. This would facilitate comparison between calculated and mea-

sured dispersion for frequencies below 30 GHz; a frequency range of great technological importance.

To get a complete description of the dispersion valid for all gas pressures the Voigt dispersion function should be used by the computer code. This requires the development of a fast numerical integration algorithm for the calculation of the Voigt dispersion function.

The hypothesis that the refractive index of air in the visible and infrared is the result of adding the "distant wing dispersion" due to all strong UV-transitions, should be tested by the existing modified FASCOD2. This requires that data for the relevant UV-transitions exists on the HITRAN data base, and a change in FASCOD2 of the maximum distance from the line center where the effect from a line is taken into account. The result of this line by line calculation depends heavily on the correctness of the Lorentzian "wings" but even a result of the same order of magnitude as given by the Edlén formula would be an encouragement.

References

(1) Edlén B (1966): The refractive index of air, Metrologia 2, 71-80.

(2) Tomiyama K, Clough S A, Kneizys F X (1987): Complex susceptibility for collisional broadning, Appl Opt 26, 2020-8.

(3) Liebe H J (1985): An updated model for millimeter wave propagation in moist air, Radio Science 20, 1069-89.

(4) Pantell R H, Puthoff H E (1969): Fundamentals of quantum electronics, John Wiley.

(5) Van Vleck J H, Huber D L (1977): Absorption, emission and linebreadths: A semihistorical perspective, Rev Mod Phys 49, 939-59.

(6) Clough S A, Kneizys F X, Rothman L S, Gallery W O (1981): Atmospheric spectral transmittance and radiance: FASCOD1B.

(7) Callen H B, Welton T A (1951): Irreversibility and generalized noise, Phys Rev 83, 34-40.

(8) Huber D L, Van Vleck J H (1966): The role of Boltzman factors in line shape, Rev Mod Phys 38, 187-205.

(9) Rothmann K (1960): Mathematische Formelsamlung, Hochschultaschenbücher Bind 13, BI-Wissenschaftsverlag.

(10) Ridgway W L et al (1982): Atmospheric transmittance/radiance computer code Fascod2, AFGL-TR-82-0392.

(11) Rothman L S et al (1987): The Hitran database, 1986 edition, Appl Opt 26, 4058-96.

(12) Hansen E R (1975): A table of series and products, Prentice-Hall.

(13) Abramowitz A, Stegun I AQ (1964): Handbook of mathematical functions, National Bureau of Standards Applied Mathematics Series 55.

A P P E N D I X A

DETAILS OF THE HILBERT TRANSFORMATION IN CHAPTER 4

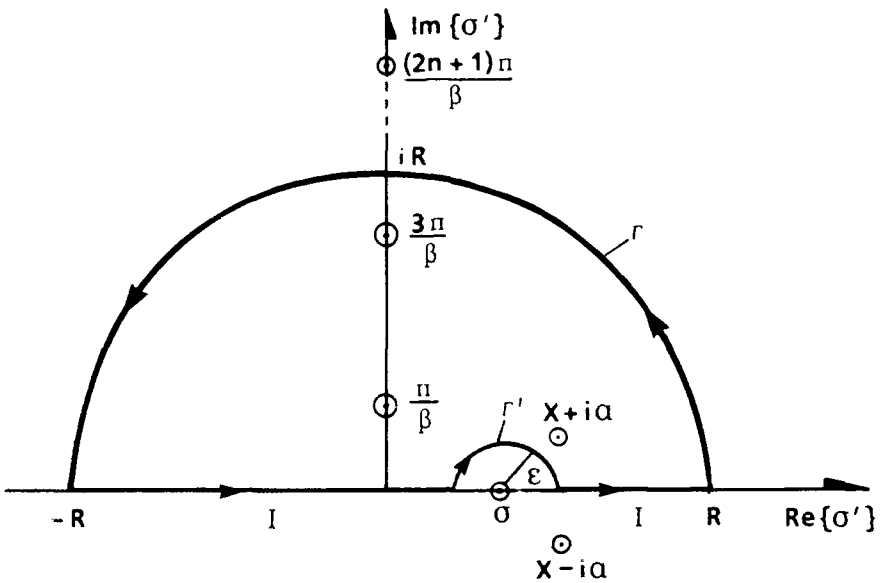

Figure A.1 The integration contour C in the complex plane which is used in the evaluation of the integral in equation (A.1). The poles of the integrand of equation (A.1) are indicated by the symbol ⊙

In Chapter 4, Equation (4.4), it was shown that in the limit where $R \to \infty$ and $\epsilon \to 0$

$$PP \int_{-\infty}^{\infty} F(\sigma')d\sigma' = 2\pi i \left\{\begin{matrix}\text{The sum of the residues of} \\ F(\sigma') \text{ inside the contour C}\end{matrix}\right\} - \lim_{\epsilon \to 0} \int_{\Gamma'} F(\sigma')d\sigma' \tag{A.1}$$

where

$$F(\sigma') = \tanh\left(\frac{\beta\sigma'}{2}\right) \frac{1}{\sigma'-\sigma} \frac{1}{\pi} \frac{\alpha}{(\sigma'-x)^2+\alpha^2} \tag{A.2}$$

$$= \tanh\left(\frac{\beta\sigma'}{2}\right) \frac{1}{\sigma'-\sigma} \frac{1}{\pi} \frac{\alpha}{\sigma'-x-i\alpha} \frac{1}{\sigma'-x+i\alpha}$$

The integration of the function in Equation (A.2) along the curve Γ'

can be evaluated as follows. The pole of $F(\sigma')$ at $\sigma'=\sigma$ is simple, so that the Laurent series has the form

$$F(\sigma') = \frac{b_1(\sigma)}{\sigma'-\sigma} + \sum_{n=0}^{\infty} a_n(\sigma'-\sigma)^n \tag{A.3}$$

By doing the substitution

$$\sigma'-\sigma = \epsilon\, e^{i\theta} \tag{A.4}$$

the integral along Γ' is given by

$$\int_{\Gamma'} F(\sigma')d\sigma' = \int_{\pi}^{0} \frac{b_1(\sigma)}{\epsilon e^{i\theta}}\, i\epsilon e^{i\theta} d\theta + \sum_{n=1}^{\infty} a_{n-1}\, \epsilon^n\, i \int_{\pi}^{0} e^{in\theta} d\theta \tag{A.5}$$

$$= -\pi i\, b_1(\sigma) + \sum_{n=1}^{\infty} a_{n-1}\, \epsilon^n\, \frac{[1-(-1)^n]}{n}$$

In the limit $\epsilon\to 0$ one gets

$$\lim_{\epsilon\to 0} \int_{\Gamma'} F(\sigma')d\sigma' = -\pi i b_1(\sigma) \tag{A.6}$$

$b_1(\sigma)$ is the residue of $F(\sigma')$ at $\sigma'=\sigma$. From Equation (A.2) this residue is given by

$$b_1(\sigma) = \operatorname*{res}_{\sigma'=\sigma} F(\sigma') = \tanh\left(\frac{\beta\sigma}{2}\right) \frac{1}{\pi} \frac{\alpha}{(\sigma-x)^2+\alpha^2} \tag{A.7}$$

In the limit $\epsilon\to 0$ the integral along Γ' is then

$$\lim_{\epsilon\to 0} \int_{\Gamma'} F(\sigma')d\sigma' = -\pi i \cdot \tanh\left(\frac{\beta\sigma}{2}\right) \cdot \frac{1}{\pi} \cdot \frac{\alpha}{(\sigma-x)^2+\alpha^2} \tag{A.8}$$

To evaluate the integral in Equation (A.1) the sum of the residues of $F(\sigma')$ inside contour C remains to be determined.

One of the poles inside the curve C is a simple pole at $\sigma' = x+i\alpha$. The residue of $F(\sigma')$ at this point is

$$\operatorname*{res}_{\sigma'=x+i\alpha} F(\sigma') = \tanh\left(\frac{\beta(x+i\alpha)}{2}\right) \frac{-i}{2} \frac{1}{\pi} \frac{1}{(x-\sigma)+i\alpha} \tag{A.9}$$

The rest of the poles of the function $F(\sigma')$ in Equation (A.2) inside the closed contour C lie on the imaginary axes. These poles are

infinitly many, simple, and they steem from the factor tanh $(\beta\sigma')/2$ in $F(\sigma')$. This factor is singular when

$$\frac{\beta\sigma'}{2} = i\,\frac{\pi}{2}\,(2n+1), \qquad n = 0,\ 1,\ 2,\ \ldots \tag{A.10}$$

The residue of pole number n is

$$\operatorname*{res}_{\sigma'=i\frac{2n+1}{\beta}\pi} F(\sigma') = \frac{2}{\beta}\,\frac{1}{i\frac{2n+1}{\beta}\pi-\sigma}\cdot\frac{\alpha}{(i\frac{2n+1}{\beta}\pi-x)^2+\alpha^2} \tag{A.11}$$

Note that this sequence of residues goes as n^{-3} for big n, so that the corresponding sum of residues converges. To find an explicit expression for the series one can use partial fraction decomposition and the relation (12)

$$\sum_{n=0}^{\infty}\frac{1}{(n+a)(n+b)} = \frac{1}{b-a}\{\psi(b)-\psi(a)\} \tag{A.12}$$

where $\psi(z)$ is the digamma function which is defined by

$$\psi(z) = \frac{d}{dz}\,(\ln\Gamma(z)) = \frac{\Gamma'(z)}{\Gamma(z)} \tag{A.13}$$

$\Gamma(z)$ is the gamma function (9).

The sum of the residues on the imaginary axis is after some algebra

$$\sum_{n=0}^{\infty}\operatorname*{res}_{\sigma'=i\frac{2n+1}{\beta}\pi} F(\sigma') =$$

$$\frac{1}{2\pi}\left[\frac{1}{\pi}\,\frac{1}{(\sigma-x)+i\alpha}\,\psi(\tfrac{1}{2}+\frac{i\beta}{2\pi}\,(x-i\alpha)) - \frac{1}{\pi}\,\frac{1}{(\sigma-x)-i\alpha}\,\psi(\tfrac{1}{2}+\frac{i\beta}{2\pi}(x+i\alpha))\right.$$

$$\left. + \frac{1}{\pi}\,\frac{2i\alpha}{(\sigma-x)^2+\alpha^2}\,\psi\,(\tfrac{1}{2}+\frac{i\beta}{2\pi}\,\sigma)\right] \tag{A.14}$$

By using the Equations (A.8), (A.9) and (A.14) the result of the integration is

$$PP\int_{-\infty}^{\infty} F(\sigma')d\sigma' = \pi i\left[\tanh\left(\frac{\beta\sigma}{2}\right)\frac{1}{\pi}\frac{\alpha}{(\sigma-x)^2+\alpha^2}\right]$$

$$+\pi\left[\tanh\left(\frac{\beta(x+i\alpha)}{2}\right)\frac{1}{\pi}\frac{1}{(x-\sigma)+i\alpha}\right]$$

$$+ i\left[\frac{1}{\pi}\frac{1}{(\sigma-x)+i\alpha}\psi(\tfrac{1}{2}+\frac{i\beta}{2\pi}(x-i\alpha)) - \frac{1}{\pi}\frac{1}{(\sigma-x)-i\alpha}\psi(\tfrac{1}{2}+\frac{i\beta}{2\pi}(x+i\alpha))\right.$$

$$\left.+\frac{1}{\pi}\frac{2i\alpha}{(\sigma-x)^2+\alpha^2}\psi(\tfrac{1}{2}+\frac{i\beta}{2\pi}\sigma)\right] \qquad (A.15)$$

The principal part of the integral evaluated is by definition a real function, but a brief look at the right hand side of (A.15) can hardly convince anyone that this is so. By rewriting (A.15) using the following relations (13)

$$\mathrm{Im}\{\psi(\tfrac{1}{2}+iy)\} = \tfrac{1}{2}\pi\tanh(\pi y) \qquad (A.16)$$

$$\psi(1-z) - \psi(z) = \pi\,\mathrm{cotg}\,\pi z \qquad (A.17)$$

$$\psi(z^*) = \psi^*(z) \qquad (A.18)$$

the result in (A.19) is obtained after some cumbersome algebra

$$PP\int_{-\infty}^{\infty} F(\sigma')d\sigma' =$$

$$\frac{1}{\pi}\frac{x-\sigma}{(x-\sigma)^2+\alpha^2}\left[\pi\frac{\sinh(\beta x)}{\cosh(\beta x)+\cos(\beta\alpha)} + \mathrm{Im}\{\psi(\tfrac{1}{2}+\frac{i\beta}{2\pi}(x-i\alpha))-\psi(\tfrac{1}{2}+\frac{i\beta}{2\pi}(x+i\alpha))\}\right]$$

$$+\frac{1}{\pi}\frac{\alpha}{(x-\sigma)^2+\alpha^2}\left[\pi\frac{\sin(\beta\alpha)}{\cosh(\beta x)+\cos(\beta\alpha)} + \mathrm{Re}\{\psi(\tfrac{1}{2}+\frac{i\beta}{2\pi}(x-i\alpha))+\psi(\tfrac{1}{2}+\frac{i\beta}{2\pi}(x+i\alpha))\}\right.$$

$$\left.-2\mathrm{Re}\{\psi(\tfrac{1}{2}+\frac{i\beta}{2\pi}\sigma)\}\right] \qquad (A.19)$$

The result in (A.19) is obviously a real function.

A P P E N D I X B

NEGLECTING THE DIGAMMA FUNCTIONS

In order to reduce the computational burden in the computation of the Lorentz dispersion function it is necessary to establish an approximation where the digamma functions can be neglected. The Lorentz dispersion function defined by Equation (5.2) is:

$$F_{\ell}(\sigma,\sigma_i) =$$

$$\frac{1}{\pi}\ \frac{\sigma_i-\sigma}{(\sigma_i-\sigma)^2+\alpha^2}\left[\frac{\sinh(\beta\sigma_i)}{\cosh(\beta\sigma_i)+\cos(\beta\alpha)}+\frac{1}{\pi}\ \mathrm{Im}\{\psi(\tfrac{1}{2}+\tfrac{i\beta}{2\pi}(\sigma_i-i\alpha))-\psi(\tfrac{1}{2}+\tfrac{i\beta}{2\pi}(\sigma_i+i\alpha))\}\right.$$

$$+\frac{1}{\pi}\ \frac{\alpha}{(\sigma_i-\sigma)^2+\alpha^2}\left[\frac{\sin(\beta\alpha)}{\cosh(\beta\sigma_i)+\cos(\beta\alpha)}+\frac{1}{\pi}\ \mathrm{Re}\{\psi(\tfrac{1}{2}+\tfrac{i\beta}{2\pi}(\sigma_i-i\alpha))+\psi(\tfrac{1}{2}+\tfrac{i\beta}{2\pi}(\sigma_i+i\alpha))\right.$$

$$\left.\left.-\frac{2}{\pi}\ \mathrm{Re}\{\psi(\tfrac{1}{2}+\frac{i\beta}{2\pi}\sigma)\}\right]\right] \qquad (B.1)$$

The desired approximation is:

$$F_{\ell A}(\sigma,\sigma_i) = \frac{1}{\pi}\ \frac{\sigma_i-\sigma}{(\sigma_i-\sigma)^2+\alpha^2}\ \frac{\sinh(\beta\sigma_i)}{\cosh(\beta\sigma_i)+\cos(\beta\alpha)}$$

$$+\frac{1}{\pi}\ \frac{\alpha}{(\sigma_i-\sigma)^2+\alpha^2}\ \frac{\sin(\beta\alpha)}{\cosh(\beta\sigma_i)+\cos(\beta\alpha)} \qquad (B.2)$$

Note that the peak value of the second term in equation (B.2) will only be of the same order of magnitude as the peak value of the first term when the resonance wave number is small. However the wave number dependence of the second term is such that it will always be unequal to zero when the first term equals zero. This is why the second term is kept for all resonance wave numbers.

The purpose of this appendix is to find the domain of resonance wave number and thermodynamic parameters where the approximation (B.2) is valid. In order to compare Equation (B.1) with Equation (B.2) the

factors containing the digamma functions in (B.1) are expanded in Taylor series.

$$\frac{1}{\pi}\,\mathrm{Im}\,\{\psi(\tfrac{1}{2}+\tfrac{\beta\alpha}{2\pi}+i\tfrac{\beta}{2\pi}\sigma_i)-\psi(\tfrac{1}{2}-\tfrac{\beta\alpha}{2\pi}+i\tfrac{\beta}{2\pi}\sigma_i)\}=$$

$$\frac{1}{\pi}\frac{d}{dx}\mathrm{Im}\,\{\psi(x+i\tfrac{\beta}{2\pi}\sigma_i)\}_{x=\frac{1}{2}}\left[\tfrac{\beta\alpha}{2\pi}-(-\tfrac{\beta\alpha}{2\pi})\right]+0\,((\tfrac{\beta\alpha}{2\pi})^2) \qquad (B.3)$$

and

$$\frac{1}{\pi}\,\mathrm{Re}\,\{\psi(\tfrac{1}{2}+\tfrac{\beta\alpha}{2\pi}+i\tfrac{\beta}{2\pi}\sigma_i)+\psi(\tfrac{1}{2}-\tfrac{\beta\alpha}{2\pi}+i\tfrac{\beta}{2\pi}\sigma_i)-2\psi(\tfrac{1}{2}+i\tfrac{\beta\sigma}{2\pi})\}=$$

$$0((\tfrac{\beta\alpha}{2\pi})^2)+\frac{2}{\pi}\frac{d}{dy}\mathrm{Re}\,\{\psi(x+iy)\}_{\substack{x=\frac{1}{2}\\ y=\frac{\beta}{2\pi}\sigma_i}}\cdot\frac{\beta}{2\pi}(\sigma_i-\sigma)+0((\sigma_i-\sigma)^2) \qquad (B.4)$$

The Figures (B.1) and (B.2) show that

$$-3\le\frac{d}{dx}\,\mathrm{Im}\,\{\psi(x+iy)\}_{x=\frac{1}{2}}<0\quad\text{when}\quad y\ge 0 \qquad (B.5)$$

This means that

$$-\frac{3\beta\alpha}{\pi^2}\le\frac{1}{\pi}\,\mathrm{Im}\,\{\psi(\tfrac{1}{2}+\tfrac{\beta\alpha}{2\pi}+i\tfrac{\beta}{2\pi}\sigma_i)-\psi(\tfrac{1}{2}-\tfrac{\beta\alpha}{2\pi}+i\tfrac{\beta}{2\pi}\sigma_i)\}<0 \qquad (B.6)$$

for all resonance wave numbers σ_i.

The second term in the first [·] in Equation (B.1) is then negligible compared to the first term when

$$\frac{\sinh(\beta\sigma_i)}{\cosh(\beta\sigma_i)+\cos(\beta\alpha)}\gg 3\,\frac{\beta\alpha}{\pi^2} \qquad (B.7)$$

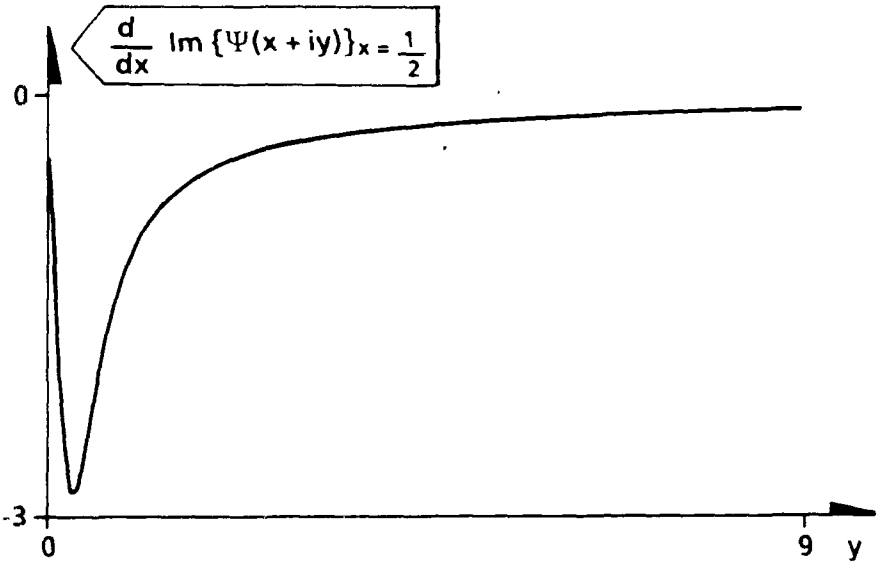

Figure B.1 The function $\frac{d}{dx}\ \mathrm{Im}\{\psi(x + iy)\}_{x=½}$ when $0 \leq y \leq 9$

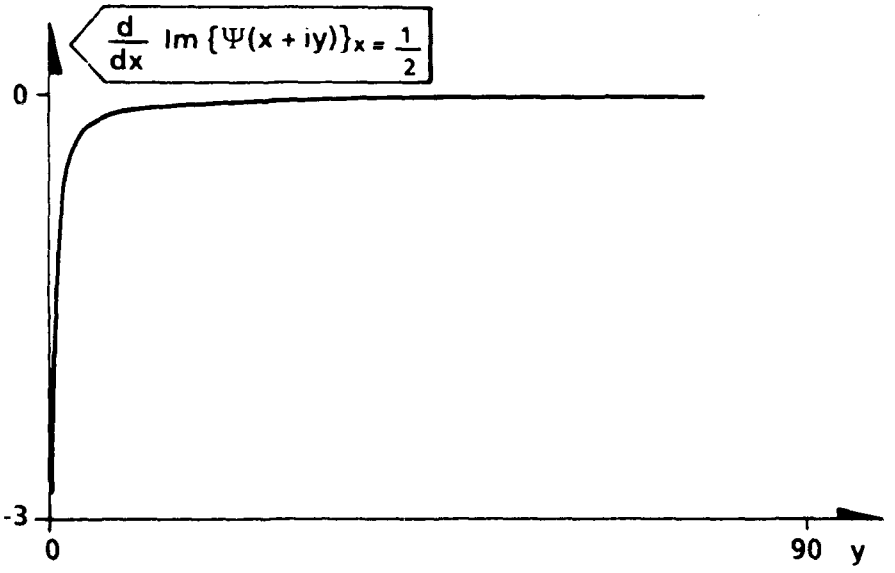

Figure B.2 The function $\frac{d}{dx}\ \mathrm{Im}\{\psi(x + iy)\}_{x=½}$ when $0 \leq y \leq 90$

The Figures (B.3) and (B.4) show that

$$0 \leq \frac{d}{dy} \text{Re}\{\psi(x + i\,y)\}_{x=\frac{1}{2}} < 3 \quad \text{when} \quad y \geq 0 \tag{B.8}$$

which implies that

$$0 \leq \frac{1}{\pi} \text{Re}\left\{\psi\left(\tfrac{1}{2} + \frac{\beta\alpha}{2\pi} + i\,\frac{\beta}{2\pi}\,\sigma_i\right) + \psi\left(\tfrac{1}{2} - \frac{\beta\alpha}{2\pi} + i\,\frac{\beta}{2\pi}\sigma_i\right) - 2\psi\left(\tfrac{1}{2} + i\frac{\beta\sigma}{2\pi}\right)\right\} < \frac{3\beta(\sigma_i - \sigma)}{\pi^2} \tag{B.9}$$

The fourth term in Equation (B.1) is then neglible compared to the first term in (B.1) when

$$\frac{\sigma_i - \sigma}{(\sigma_i - \sigma)^2 + \alpha^2} \cdot \frac{\sinh(\beta\sigma_i)}{\cosh(\beta\sigma_i) + \cos(\beta\alpha)} \gg \frac{\alpha}{(\sigma_i - \sigma)^2 + \alpha^2} \cdot \frac{3\beta(\sigma_i - \sigma)}{\pi^2} \tag{B.10}$$

A simplification of Equation (B.10) yields

$$\frac{\sinh(\beta\sigma_i)}{\cosh(\beta\sigma_i) + \cos(\beta\alpha)} \gg \frac{3\beta\alpha}{\pi^2} \tag{B.11}$$

Since the Equations (B.7) and (B.11) are identical the digamma functions in (B.1) can be neglected when Equation (B.11) is satisfied.

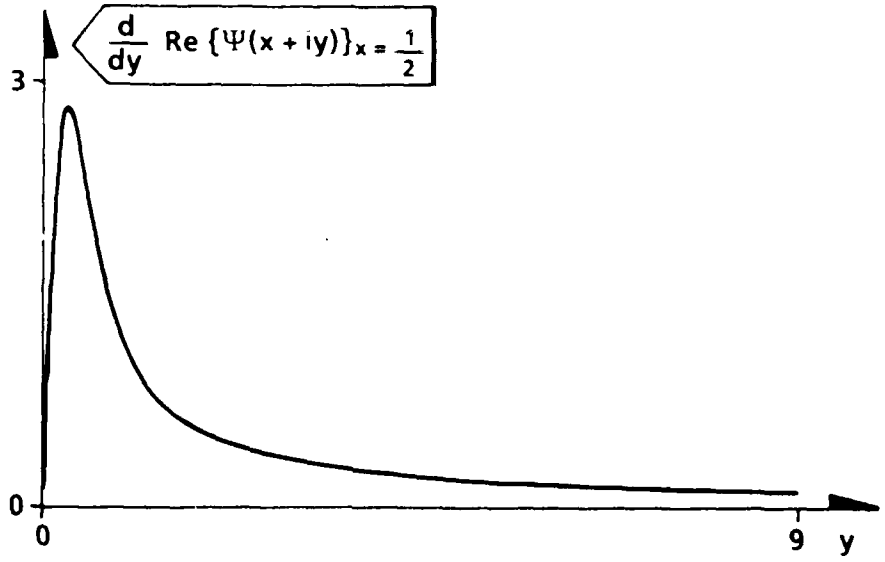

Figure B.3 The function $\frac{d}{dy}\,\text{Re}\{\psi(x + iy)\}_{x=\frac{1}{2}}$ when $0 \leq y \leq 9$

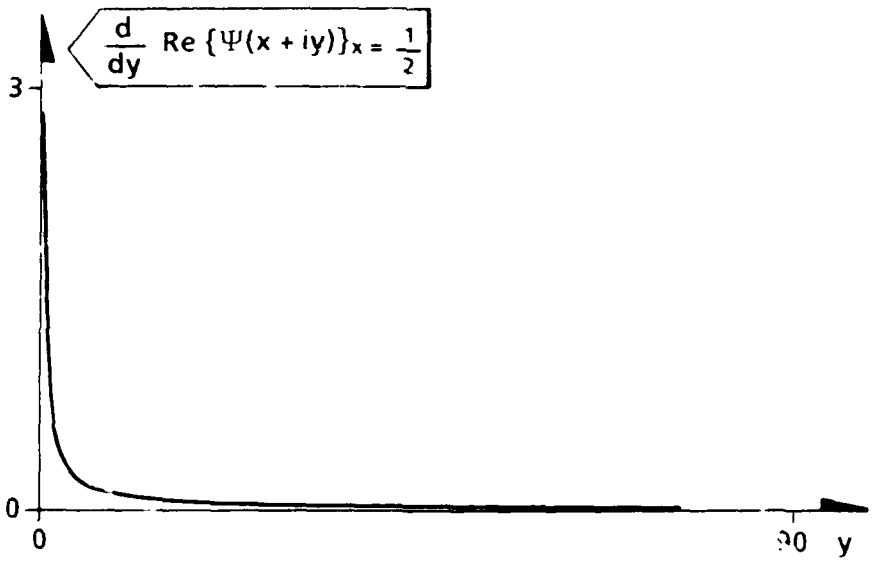

Figure 8.4 The function $\frac{d}{dy}$ $Re\{\psi(x + iy)\}_{x=½}$ when $0 \leq y \leq 90$

A P P E N D I X C

AN OVERVIEW OF ATMOSPHERIC DISPERSION IN THE WAVE NUMBER INTERVAL 500-15000 cm^{-1}

This Appendix gives an overview of calculated atmospheric dispersion in the wave number interval 500-15000 cm^{-1}. The atmospheric model used in these calculations is the Midlatitude summer model, (pressure 1013 mb, temperature 294 K).

The interval (0-500) cm^{-1} is not presented here because Figure 6.1 covers this spectral range. The interval 15000-17900 cm^{-1} is not shown because the dispersion is very small in this region ($<<10^{-9}$).

Each figure covers a broad interval of wave numbers. These figures therefore gives only an impression of the magnitude of the dispersion in the different wave number intervals. The dispersion varies about four orders of magnitude throughout the wave number interval; from about 10^{-5}-10^{-9}.

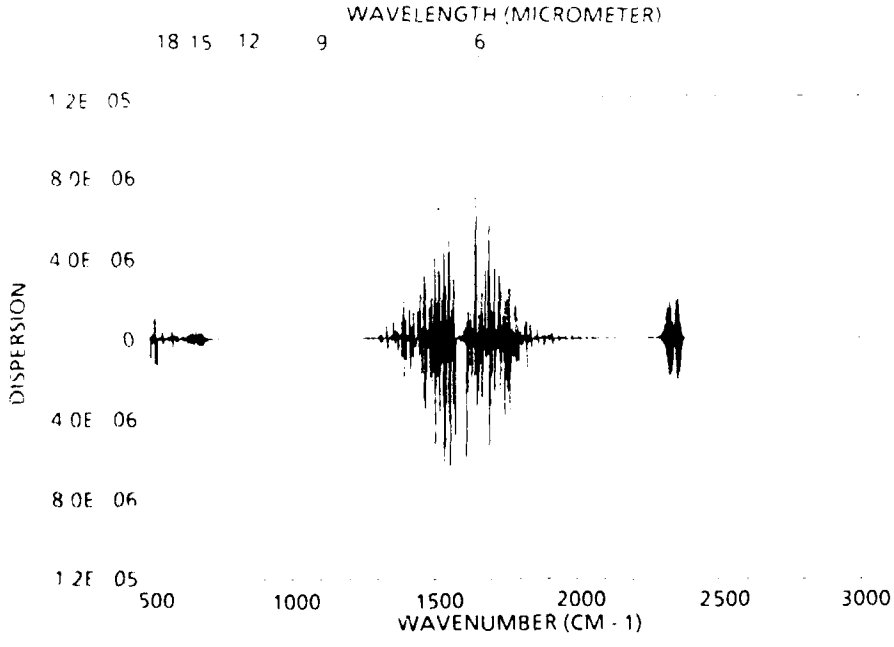

Figure C.1 The atmospheric dispersion for the wave number interval 500-3000 cm^{-1}. Midlatitude summer

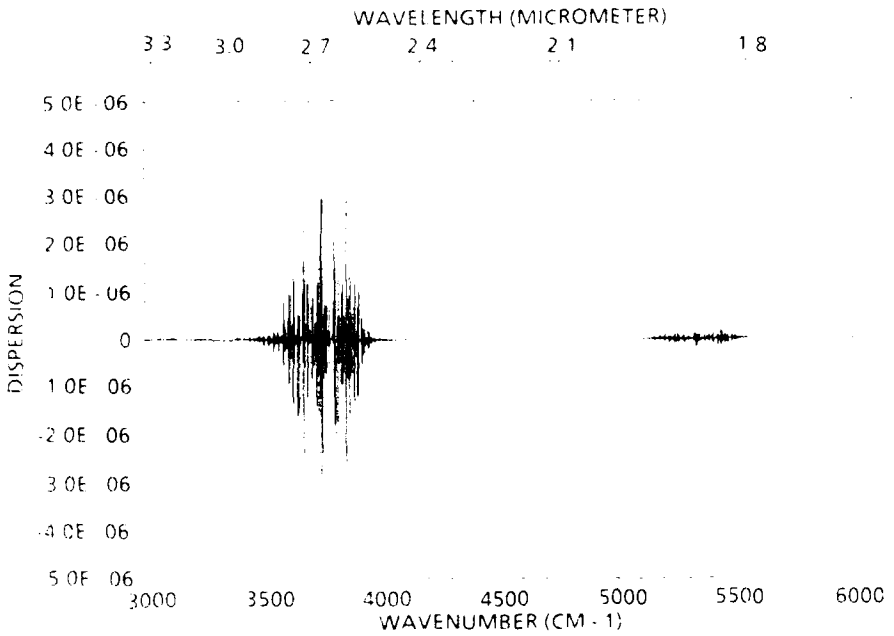

Figure C.2 The atmospheric dispersion for the wave number interval 3000-6000 cm^{-1}. Midlatitude summer

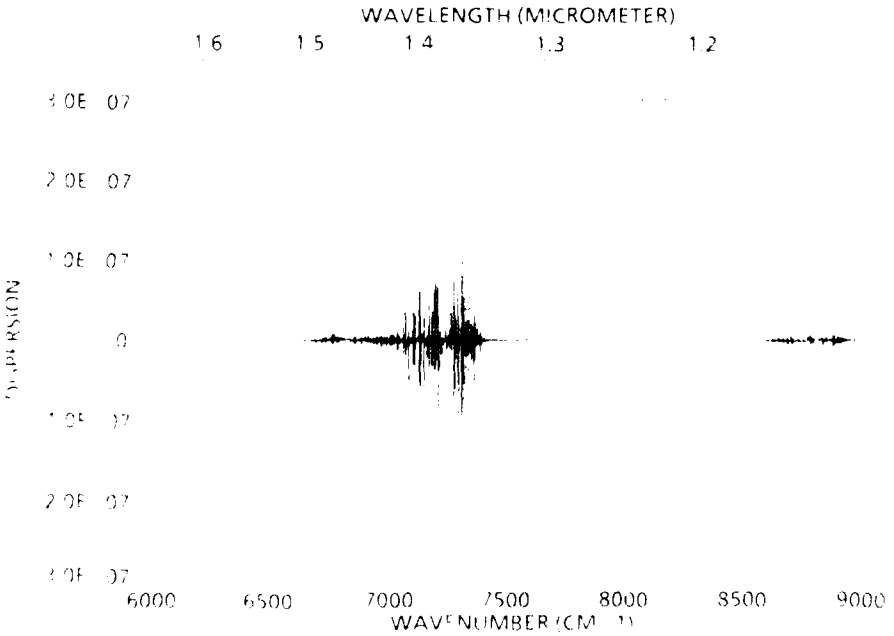

Figure C.3 The atmospheric dispersion for the wave number interval 6000-9000 cm^{-1}. Midlatitude summer

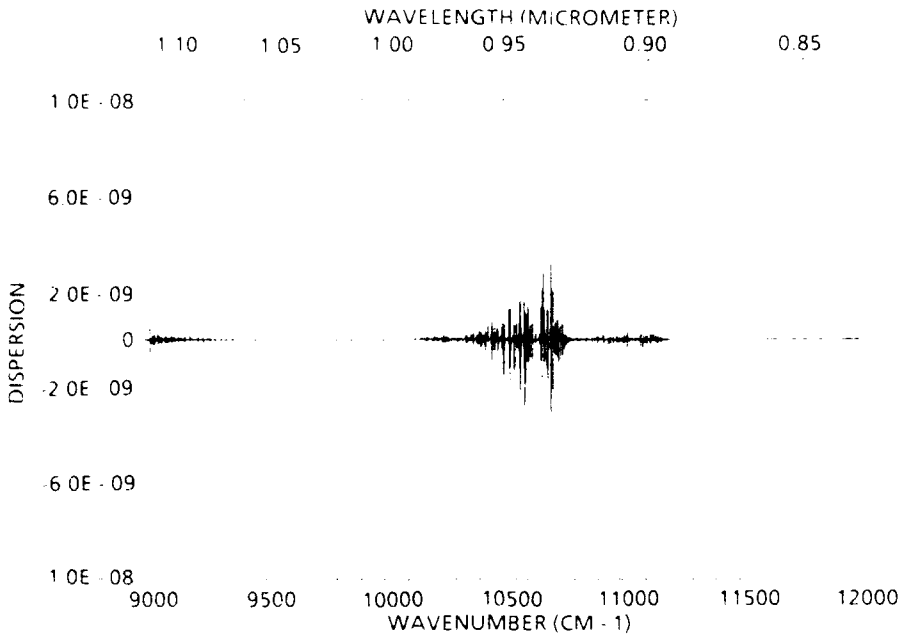

Figure C.4 The atmospheric dispersion for the wave number interval 9000-12000 cm^{-1}. Midlatitude summer

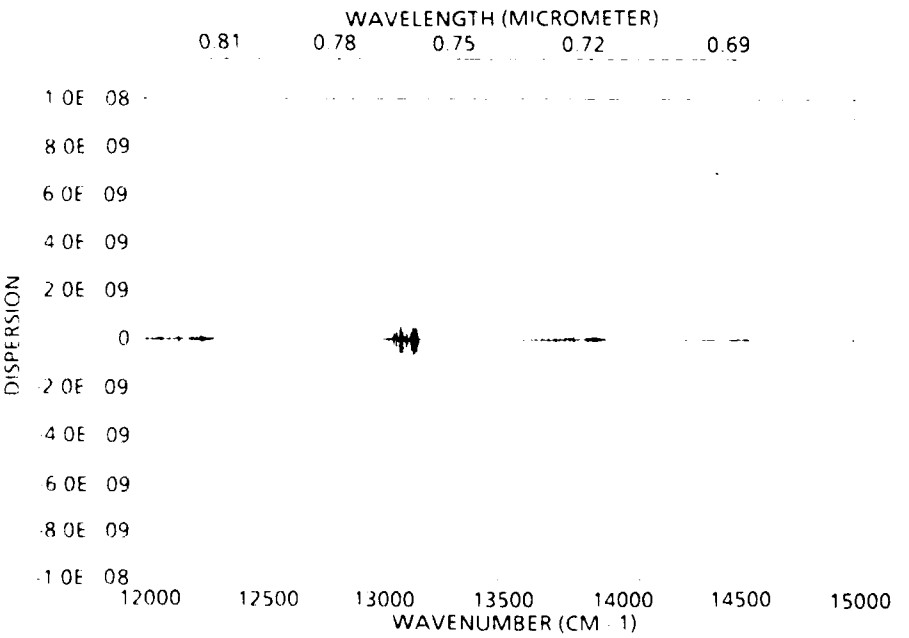

Figure C.5 The atmospheric dispersion for the wave number interval 12000-15000 cm^{-1}. Midlatitude summer